https://doi.org/10.5194/egusphere-2026-687
Preprint. Discussion started: 5 March 2026

Isotopic Evidence for Ice Growth by Riming in Precipitation

Pradeep K. Aggarwal[1], Courtney Schumacher[2], Frederick J. Longstaffe[3], Aaron Funk[2], Matthew D. Shupe[4,5]

[1]International Atomic Energy Agency, A1400, Vienna, Austria (retired)
[2]Department of Atmospheric Sciences, Texas A&M University, College Station, TX 77843, USA
[3]Department of Earth Sciences, The University of Western Ontario, London, Ontario, N6A 5B7, Canada
[4]Cooperative Institute for Research in Environmental Sciences, University of Colorado, Boulder, CO 80302, USA
[5] NOAA Physical Sciences Laboratory, Boulder, CO 80305, USA

Correspondence to: Pradeep K. Aggarwal (pkaggarwal@gmail.com)

Submitted to: **Atmospheric Chemistry and Physics**

February 4, 2026

Abstract. In this study, we investigate the impact of riming on the relative composition of oxygen and hydrogen isotopes or d-excess in precipitation. Riming, where supercooled liquid droplets freeze directly on ice particles, is an important process of precipitation formation in mixed-phase clouds but has long been assumed to occur without isotopic fractionation. We used an independent indicator of riming, the terminal fall velocity of snow particles, and correlated it with the d-excess of snow or rain precipitation (ranging from –23 to +45‰) in polar (Arctic, Antarctic), mid-latitude and tropical regions. Our results show an inverse correlation of d-excess with terminal fall velocity, which increases with riming, indicating that lower d-excess reflects variable extents of riming during precipitation formation. The lower d-excess of rimed ice results from a partial loss of the accreted liquid by evaporation, and possibly splashing and shedding, before freezing is complete. This contrasts with a higher d-excess of ice that grows by the vapor deposition process. We conclude that low d-excess from riming can explain the spatial variations of Greenland and Antarctica surface snow that were previously attributed to changes in source moisture origin. Our results also help to explain the wide range of d-excess observed in daily precipitation compared to a much narrower range in surface snow or ice cores. Further, spatial or temporal differences in d-excess would allow for the estimation of variations in the rimed mass fraction, which, in turn, can be used as observational constraints for improving microphysics schemes in climate models.

https://doi.org/10.5194/egusphere-2026-687
Preprint. Discussion started: 5 March 2026

1 Introduction

Polar ice cores have long been known to record temperature changes in past climates based on their oxygen ($\delta^{18}O$) and hydrogen ($\delta^{2}H$) isotope compositions (e.g., Dansgaard et al., 1969; Jouzel et al., 2013). The relative composition of these isotopes, namely d-excess (defined as $\delta^{2}H - 8\delta^{18}O$), is believed to provide insights into the climatic conditions (temperature, relative humidity, windspeed) of source moisture origin (Dansgaard, 1964; Masson-Delmotte et al., 2005; Jouzel et al., 2013). Lower d-excess of Greenland and Antarctic ice cores from the Last Glacial Maximum (LGM) compared to the Holocene, or in the warming phase compared to the cooling phase of abrupt climate change events in Greenland (Jouzel et al, 2007), are suggested to indicate substantial and rapid reorganization of the high-latitude hydrological cycles that changes the geographical region of source moisture origin (Johnson et al., 1989; Jouzel et al., 2007). In addition to temporal differences, increasing d-excess of surface snow from the south to the north of Greenland is attributed to differences in source moisture origin (Johnson et al., 1989; Masson-Delmotte et al., 2005).

The interpretation of the d-excess of precipitation and ice cores is guided by two primary constraints (Fig. S1, Supplementary Material). The first constraint is that lower d-excess values (less than the observed global average of ~10‰; Dansgaard, 1964) are inherited from the oceanic source moisture (Dansgaard, 1964; Merlivat and Jouzel, 1979; Johnsson et al., 1989). This is because isotopic fractionation during evaporation results in a lower d-excess of the vapor than the liquid (Dansgaard, 1964). The magnitude of this fractionation increases (i.e., the d-excess of the vapor is lower) when evaporation occurs under higher humidity, cooler temperature, and/or higher windspeed conditions (Dansgaard, 1964; Merlivat and Jouzel, 1979). Under the current climate, a d-excess range of ~3 to 5‰ is estimated for vapor originating from ocean evaporation in the southern and northern hemispheres (Pfahl and Sodemann, 2014).

The second constraint is related to ice growth in mixed phase clouds, where a supercooled liquid phase co-exists with ice and vapor at temperatures above approximately –40°C (Pruppacher and Klett, 2010; Houze, 2014); there, when ice crystals grow by the vapor deposition or Wegener-Bergeron-Findeisen (WBF) process, they have a higher d-excess. In the WBF process, liquid droplets do not come in direct contact with the ice particles, but instead evaporate owing to a higher saturation vapor pressure over liquid than ice. The vapor then diffuses and is deposited on ice particles (Houze, 2014; Pruppacher and Klett, 2010). A large isotopic fractionation during deposition growth results in a d-excess of ice that is ~30‰ or more, higher than that of the liquid, depending upon the level of supersaturation in the vapor with respect to ice (Jouzel and Merlivat, 1984; Uemura et al., 2005; Casado et al., 2016).

As the increase in d-excess during ice growth by vapor deposition is much larger than the range of lower values resulting from source moisture differences, the influence of source moisture on d-excess may be important when precipitation forms as “warm rain” that does not involve freezing. Most precipitation over land and oceans, however, originates as snow

https://doi.org/10.5194/egusphere-2026-687
Preprint. Discussion started: 5 March 2026

(Mülmenstädt et al., 2015; Field and Heymsfield, 2015). The snow either falls to the Earth's surface without melting or melts below the 0°C level to reach the surface as rainfall. This implies that source moisture origin may only have a limited influence globally, and the lower d-excess of precipitation must result from an alternative mechanism.

Ice growth in mixed phase clouds can also occur by riming. The riming process, in contrast to WBF, involves the collision of liquid droplets and ice particles and the direct freezing of the droplets on the particle surface (Pruppacher and Klett, 2010; Houze, 2014). A fundamental assumption in existing interpretations of d-excess is that unlike vapor deposition, there is no isotopic fractionation during riming (Federer et al., 1982; Merlivat and Jouzel, 1984; Ciais and Jouzel, 1994; Bailey et al., 2025). That is, the rimed ice has the same isotopic composition and d-excess as the liquid. To the best of our knowledge, this assumption has not been thoroughly explored in the literature.

Evidence from field, laboratory and modeling studies suggests that isotopic fractionation may indeed be involved in riming. For example, analyses of freshly fallen snow in the Sierra Nevada and Rocky Mountains show that the $\delta^{18}O$ values increase as riming increases (Demoz et al., 1991; Lowenthal et al., 2011; Lowenthal et al., 2016). Bailey et al. (1969) conducted laboratory experiments to study the isotopic fractionation in riming and found that the $\delta^{18}O$ and $\delta^{2}H$ values of the frozen material were slightly higher than those of the supercooled liquid. The higher δ values were attributed to evaporation of the accreted liquid before freezing was complete. A modeling study by Jouzel et al. (1985) corroborated the laboratory results and suggested that the higher δ values of the rimed ice result from the evaporation of the accreted liquid and/or its partial freezing. These laboratory and modeling studies were conducted in the context of hailstone formation. Hailstones are an extreme case of riming, distinguished only by their much larger size (>5 mm) compared to rimed particles (Pruppacher and Klett, 2010). A continuum of ice particles from unrimed to graupel and hail has been shown based on their mass-size relationships (Lin and Colle, 2011).

More significantly than the slightly higher δ values, the d-excess of rimed ice in the laboratory and modeling studies was much lower than that of the supercooled liquid. Natural hailstones analysed by Jouzel et al. (1985) had low (<10‰) values of d-excess. Increased riming in snow from the Rocky Mountains (Lowenthal et al., 2016) also appears to correspond to lower d-excess values.

A lower d-excess of rimed ice is consistent with the mechanism of riming growth that involves evaporation and partial loss of the accreted water (e.g., Macklin and Payne, 1967; Pruppacher and Klett, 2010 and references therein). Briefly, when a liquid droplet collides with an ice particle, it may lose some of the water by splashing, depending on the impact velocity. The drop initially freezes with a thin frozen shell as the latent heat of fusion released in the process warms the inner part of the droplet. The colliding droplet may also spread to form a thin film on the particle surface. Heat dissipation then occurs by

https://doi.org/10.5194/egusphere-2026-687
Preprint. Discussion started: 5 March 2026

conduction, raising the particle surface temperature to be higher than that of the surrounding air, and by evaporation when the air is subsaturated with water vapor. If the latent heat is dissipated fast enough to keep the particle surface temperature a few degrees below 0°C, the accreted water may freeze in a "dry" growth regime. Conversely, if dissipation is slower, for example due to high droplet population or increased frequency of droplet-particle collisions, the particle surface temperature may rise to 0°C. In that case, the accreted water freezes in a "wet" growth regime and some of the water may be lost by shedding, in addition to evaporation, before freezing is complete. The water loss by splashing, shedding, and evaporation may be as much as 30% or higher, depending upon the structure of the ice crystals, impact velocity of droplets, and other physical parameters (Pruppacher and Klett, 2010).

Riming is ubiquitous under a variety of meteorological conditions, throughout the year and at all latitudes (Korolev et al., 2017). It is estimated that in mixed phase regions, the riming process is active in about half of the stratiform clouds, and almost all of the convective clouds. For example, about 30 to 50% of the surface snowfall mass in the Sierra Nevada Mountains (Mitchell et al., 1990; Lowenthal et al., 2011) and near Sapporo, Japan (Harimaya and Sato, 1989) is estimated to result from riming. Arctic precipitation at Hyytiälä, Finland or Ny-Ålesund, Svalbard includes up to 40% of the snow mass from riming (Moiseev et al., 2017; Chellini and Kneifel, 2024). At Oliktok Point, Alaska, USA, about two thirds of the Arctic precipitation forms by riming that is heavier during the winter than the summer (Fitch and Garret, 2022). Riming has been observed in snowfall on the South Pole (Ohtake, 1978). In eastern Antarctic coastal precipitation at Dumont d'Urville, a mean riming growth of about 30% was estimated with ~11% of the rimed particles being fully developed graupel (Grazioli et al., 2017).

Riming increases the particle mass and density and it becomes more rounded in shape (Pruppacher and Klett, 2010; Houze, 2014). These changes result in a generally higher terminal fall velocity of rimed particles compared to that of unrimed particles, which grow by vapor deposition (Locatelli and Hobbs, 1974; Weiss et al., 1977; Heymsfield and Kajikawa, 1987; Pruppacher and Klett, 2010; Heymsfield et al., 2013; Garret and Yuter, 2014; Houze, 2014; Kneifel and Moisseev, 2020; Matrosov, 2023). Smaller rimed particles may in some cases have a similar or lower fall velocity compared to larger unrimed particles such as aggregates (Locatelli and Hobbs, 1974). Aggregates are formed by the collision of ice crystals, which themselves may have grown by the WBF or the riming process. While the fall velocity of aggregates or other particles is dependent on physical characteristics (size, shape, mass and density), the d-excess would respond to the microphysical process (WBF or riming) responsible for phase change from liquid to ice.

In this study, we use the terminal fall velocity as an independent parameter to explore the impact of riming on d-excess in polar to tropical precipitation (observed d-excess range ~ –23 to +45‰). We have also used photographic images of precipitating snowflakes to document riming at one of the polar locations in our study. Our findings reveal that precipitation d-excess values decrease with increasing terminal fall velocity or the fraction of particle mass attributed to riming. We

https://doi.org/10.5194/egusphere-2026-687
Preprint. Discussion started: 5 March 2026

conclude that d-excess is a powerful indicator of riming in precipitation and that d-excess variations in ice cores should be reevaluated with respect to the microphysical processes of snow formation, which in turn reflect a change in cloud dynamics.

2 Data and Methods

2.1 Study Locations

Our hypothesis is that the d-excess values reflect microphysical processes associated with riming. It is important, therefore, to consider concurrent data for isotope compositions and terminal fall velocities on a daily or shorter time scale in order to minimize data averaging much beyond the precipitation events where isotope compositions are acquired. Likewise, because the nature of cloud microphysical processes is essentially the same on the global scale (Pruppacher and Klett, 2010; Houze, 2014), it is important to consider data from the polar to the tropical regions. Fig. 1 shows the locations where we have successfully compiled concurrent isotope and terminal fall velocity data and Table 1 lists the coordinates.

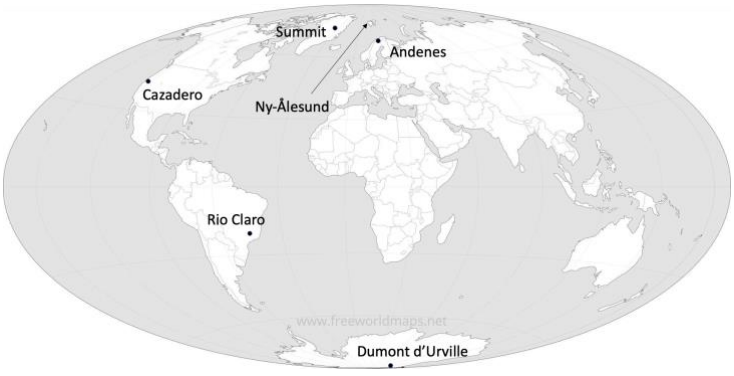

Figure 1. Map showing the study locations (base map downloaded from https://www.freeworldmaps.net/printable/hammer-worldmap-hd.jpg).

2.2 Isotope data

Isotopic compositions of precipitation were obtained from published studies. At the polar locations, precipitation samples were collected on a daily (~24 hr) time scale while those at the mid-latitude and tropical locations were collected at a higher frequency (~30 min or less). The oxygen and hydrogen isotope analyses were conducted by standard methods using mass-spectrometers or laser analyzers and the analytical details are available in the original publications. As noted previously, d-

https://doi.org/10.5194/egusphere-2026-687
Preprint. Discussion started: 5 March 2026

excess is defined as: d (‰) = $\delta^2H - 8\delta^{18}O$, where $\delta = (R_{sample} / R_{standard} - 1)$ 1000, and R is the isotope ratio ($^{18}O/^{16}O$) or ($^2H/H$) in a sample or the VSMOW (Vienna Standard Mean Ocean Water) isotope standard.

Table 1. Coordinates and surface elevations (meters above sea level) of study locations.

Location	Latitude	Longitude	Elevation (masl)
Polar			
Summit, Greenland	72° 36' N	38° 30' W	3250
Ny-Ålesund, Svalbard, Norway	78° 92' N	11° 92' E	11
Andenes, Norway	69° 14' N	15° 68' E	10
Dumont d'Urville, Antarctica	66° 39' S	140° 0' E	41
Mid-latitudes			
Cazadero, California	38° 36' N	123° 13' W	475
Tropics			
Rio Claro, Brazil	22° 39' S	47° 54' W	670

2.2.1 Summit, Greenland

Kopec et al. (2019) reported the isotopic compositions of daily precipitation between July 2011 – September 2014. The d-excess values range from +6.4 to +34.9‰ in the summer (June, July, August or JJA) and from –10.6 to +15.9‰ in the winter (December, January, February or DJF). During the other seasons, d-excess values range from –9.3 to +25.4‰. Kopec et al. (2019) attributed summer – winter d-excess differences to the source of moisture, including by sublimation of surface snow in the summer. However, relatively higher (> 10) or lower (< 10) d-excess values occur both in the summer and in the winter.

2.2.2 Ny-Ålesund and Andenes, Norway

Leroy-Dos Santos (2020) reported the isotopic compositions of daily precipitation at Ny-Ålesund, located on the west coast of Svalbard, Norway, during 2014 – 2018. Limited datasets have been reported for July – August 2018 (Mellat et al., 2021) and February – March 2020 (Seidl et al., 2024). Isotopic composition of Andenes, Norway precipitation (rain and snow) for

https://doi.org/10.5194/egusphere-2026-687
Preprint. Discussion started: 5 March 2026

February – March 2020 also was reported by Seidl et al. (2024). Daily precipitation samples were collected at both locations. In addition, sub-daily precipitation samples were collected during the 2020 campaigns. The precipitation samples at Ny-Ålesund and Andenes consisted of snow, rain and 'melt', probably referring to a mixture of rain and snow, with d-excess values ranging from –55.8 to +45.2‰. The d-excess of samples selected for this study (rain and snow), based on radar data availability, ranges from –8.6 to +45.2‰ at Ny-Ålesund and from –1.0 to 30.2‰ at Andenes.

2.2.3 Dumont d'Urville, Antarctica

The isotopic compositions of daily precipitation from January – July 2019 and January – December 2020 were reported by Leroy-Dos Santos (2023). A smaller subset of the reported data was selected based on radar data availability and after eliminating those samples that may have been affected by sublimation at lower elevations (see below). The d-excess of selected samples ranges from –5.0 to +14.0‰.

2.2.4 Cazadero, California

Coplen et al. (2015) provided the isotopic compositions of precipitation from multiple events between January to March over the 2005 – 2010 period. The precipitation samples were collected with an automated sampling device at ~30-min intervals. Several events in March 2005, February 2007, March 2009 and January 2010 were selected for this study based on the radar characteristics of precipitation with d-excess ranging from –22.9 to +20.5‰.

2.2.5 Rio Claro, Brazil

The isotopic composition of tropical rainfall at Rio Claro, Brazil was reported by Santos et al. (2024). Rainfall was sampled at 5-10 min intervals during precipitation events lasting for about an hour to several hours. Three events on 8 October 2019, 10 December 2019, and 5 January 2020 were selected for this study based on the availability of sufficient radar data (see below). The d-excess values of selected samples ranged from +4.5 to +21.9‰.

2.3 Terminal Fall Velocity

The terminal fall velocity of ice particles is commonly determined using vertically-pointing ground-based Doppler radars (Houze, 2014) or particle imaging devices such as a multi-angle snowflake camera, MASC (Garret and Yuter, 2014; Praz et al., 2017). Doppler velocities from profiling radars have been reported at each of the study locations for all or part of the same time period as the isotope samples. In addition, a limited amount of concurrent terminal fall velocity data acquired with a MASC were retrieved for Summit, Greenland.

https://doi.org/10.5194/egusphere-2026-687
Preprint. Discussion started: 5 March 2026

205

2.3.1 Doppler velocity and terminal fall speed in stratiform clouds

The use of Doppler radars for measuring the terminal fall velocities of hydrometeors has been extensively described in the literature (e.g., Weiss and Hobbs, 1975; Orr and Kropfli, 1998; Protat and Williams, 2011; Houze, 2014). Briefly, Doppler radars used for cloud and precipitation studies emit radiation that is reflected by various hydrometeors (snow, ice or rain
210 drops) and the travel time, strength, and phase of the returned signal are used to determine the altitude (or range), reflectivity, and Doppler velocity of the reflecting objects (Houze, 2014). The reflectivity values are reported as the "effective reflectivity" (Z_e) in units of $mm^6\ m^{-3}$ (or in decibels, $dBZ = 10\ \log_{10} Z_e$). The Doppler velocity is denoted as the mean Doppler velocity (MDV) with units of ms^{-1} and is the reflectivity-weighted mean of the measured Doppler spectrum. An altitude correction is applied to Doppler velocities owing to the lower air density (pressure) at higher elevations (Heymsfield
215 et al., 2013): $MDV_o = MDV_h \left(\frac{\rho_o}{\rho_h}\right)^{-0.4} \approx MDV_h \left(\frac{1000}{P_h}\right)^{-0.4}$. Here, ρ is air density, P is atmospheric pressure, and the subscripts o and h, respectively, are mean sea level or the height where measurement is made. Note that we are using the convention that positive MDV is towards the radar such that lower MDV values indicate weaker downward motion.

The mean Doppler velocity consists of two components: the terminal fall velocity of the hydrometeor (V_t) and the vertical air
220 motion (V_a): $MDV = V_t + V_a$ (Orr and Kropfli, 1999; Houze, 2014). In stratiform clouds, small-scale vertical air motions are both upwards and downwards (Orr and Kropfli, 1999; Houze, 2014). It has been shown that these small-scale air motions cancel out when MDV is averaged over a period of at least 20-30 min in stratiform or anvil cloud regions (Mosimann, 1995; Orr and Kropfli, 1999; Protat and Williams, 2011). Then, $MDV \approx V_t$. The assumption of cancelling vertical air motions is not valid for convective clouds where downdrafts and updrafts are significantly higher, such that the use of MDV for
225 characterizing the rimed nature of snow particles is only feasible for stratiform precipitation (Mosimann, 1995; Orr and Kropfli, 1999).

Terminal velocities and particle size distributions from field campaigns conducted over a wide temperature range (–86° to 0°C) were evaluated by Heymsfield et al. (2013). All else being equal (e.g., particle shape, degree of riming), the MDV (and
230 reflectivity) is lower when precipitation consists of smaller particles, which in general are produced in colder clouds. As a result, seasonal differences in particle size may mask the potential increase in MDV due to riming (Heymsfield et al., 2013; Chellini and Kneifel, 2024). In the present study, particle size effects appear to be most significant for precipitation at Summit, Greenland (Sect. 3.1.3).

https://doi.org/10.5194/egusphere-2026-687
Preprint. Discussion started: 5 March 2026

2.3.2 Doppler velocity and precipitation phase

While d-excess is measured in precipitation samples collected on the ground, the altitude at which the MDV values can be used to characterize riming depends on the phase (snow or rain) of precipitation. For snowfall, MDV close to the ground at a height free of ground interference can be used (Weiss and Hobbs, 1975; Orr and Kropfli, 1999). In the case of rainfall, however, the MDV aloft in the snow region above the melting level is used (Fig. S2).

Stratiform rain results from the melting of snow particles in an ~500 m thick layer (Fig. S2; Pruppacher and Klett, 2010; Houze, 2014). The height of the melting layer above ground is less than about 3 km in mid- to high-latitudes and less than about 5 km in the tropics. Within the melting layer, the snowflakes generally melt without further growth or breaking into smaller drops (Ohtake, 1969; Karrer et al., 2022). Weiss et al. (1977) investigated the use of MDV during rainfall to determine the rimed nature of snow particles above the melting layer. They used the fall velocity of rimed and unrimed snow particles of known mass measured in situ by Locatelli et al. (1974) as the fall velocity of snow (V_s) above the melting layer. The relationship between raindrop mass and fall velocity (Atlas et al., 1973) was used to obtain the fall velocity of raindrops just below the melting layer (V_r). Based on a correlation of V_s versus V_r, graupel and heavily rimed particles could be differentiated from unrimed or lightly rimed aggregates, as validated against field measurements (Weiss et al., 1977). Mosimann (1995) and Zawadzki et al. (2005) have also suggested that riming during rainfall can be characterized by using particle fall velocities in the snow region.

The melting layer is identified by a distinct peak in radar reflectivity or “bright band” (Fig. S2; Pruppacher and Klett, 2010; Houze, 2014). White et al. (2002) proposed that the top of the melting layer occurs above the bright band at the inflection point in the MDV gradient from nearly vertical to a gentler slope (Fig. S2). An opposite inflection characterizes the bottom of the melting layer below the bright band. We used this approach to retrieve the MDV above the melting layer at Cazadero, California and Rio Claro, Brazil where all precipitation was in the form of rainfall. The same approach was used for Ny-Ålesund and Andenes, Norway when rainfall was indicated by a bright band in the reflectivity profiles.

2.3.3 Doppler velocity at the study locations

Table 2 shows the details of Doppler radars deployed at the locations in this study along with the data sources that describe the collection and processing of raw data. The reflectivity and MDV data at very low reflectivity values (<–25 dBZ) were not considered. The dates and times of data averaging for reflectivity and MDV are provided in Table S1 and are briefly described below. We note that daily isotope sampling at the polar locations includes parts of two calendar days. To be precise, we would average the MDV over the same 24-hr period. However, radar data were not always available for two consecutive days and in some cases, there was no or little precipitation on the first day. Sensitivity testing with available data

https://doi.org/10.5194/egusphere-2026-687
Preprint. Discussion started: 5 March 2026

for 24-hr average MDV over consecutive days of precipitation indicated a negligible difference from the daily average for one calendar day.

Summit: Snowfall at Summit is generally weak (Shupe et al., 2013) and average values of reflectivity and MDV were calculated on a daily time scale, concurrent with isotope sampling. The reflectivity and terminal fall velocity at Summit increase as snow particles fall toward the ground surface, indicating continuous particle growth (Castellani, 2015; Pettersen et al., 2018). Therefore, the lowest radar level (~200 m) was used that is free of ground clutter (Shupe et al., 2013; Castellani, 2015). An air density correction was applied to MDV values as the ground elevation at Summit station is ~3200 m.

Table 2. Characteristics of Doppler radar and sources of data at the study locations

Location	Frequency (GHz)	Vertical Resolution (m)	Range (m)	Time Resolution (s)	Data Source
Summit	35	45	6000	2	ARM (2010)
Ny-Ålesund	24.1	30	930	60	Ebell et al. (2023)
Andenes	35	30	6000	2	ARM (2019)
Dumont d'Urville	24.1	100	3100	60	Wiener et al. (2024)
Cazadero	2.875	60	10162	30	Coplen et al. (2015)
Rio Claro	24.1	150 or 300	4650 or 9300	60	Santos et al. (2024)

Ny-Ålesund and Andenes: Daily averages of reflectivity and MDV were obtained for the days of interest based on isotope sampling. Radar data were available for 2017 – 2020 at Ny-Ålesund and for 2020 at Andenes. The precipitation phase was identified from the presence or absence of a bright band in vertical profiles of reflectivity. When present, the top of the bright band generally was at about 600 – 900 m above ground. As snow and rain may occur at these locations within a single day, we also evaluated sub-daily vertical profiles in the 0 – 12 hr and 12 – 24 hr time intervals. In many cases, the bright band occurred only in one interval and the radar reflectivity and MDV profiles generally were not usable for correlation with the daily values of d-excess, except for some of the 2020 samples that were collected at sub-daily intervals (Table S1). These constraints on radar data did not allow for the use of the lowest d-excess samples (< –10‰) in this study. For snow precipitation, the 150-m level above ground was used to avoid ground interference with the radar measurements at lower levels.

https://doi.org/10.5194/egusphere-2026-687
Preprint. Discussion started: 5 March 2026

Dumont d'Urville: All precipitation at this location is stratiform (Wiener et al., 2024) and daily averages of reflectivity and MDV were calculated. These values increase with decreasing altitude up to about 1 km above ground, consistent with snow particles growing as they fall towards the ground surface. At lower heights, sub-cloud sublimation of snow may be significant due to strong katabatic winds blowing off of the Antarctic continent (Grazioli et al., 2017; Wiener et al., 2024).

Sublimation decreases the reflectivity of snow at lower altitudes (Duran-Alarcon et al., 2019). Katabatic winds may consistently increase the Doppler velocity (Wiener et al., 2024) and it may no longer be equated with the terminal fall velocity. We used the vertical profiles of reflectivity below 2.5 km to exclude sublimation-affected data (Duran-Alarcon et al., 2019). The profiles could be classified in two groups. One group shows a substantial decrease below ~1 km that indicates sublimation (Fig. S3). In the second group, reflectivity below ~1 km did not change significantly and the MDV values were retrieved for the 300-m level, which is the lowest level at this location free of ground interference with radar measurements (Wiener et al., 2024).

Cazadero: The radar reflectivity and Doppler velocity data for several precipitation events between 2005-2010 were available. We selected the time intervals where a bright band was clearly present and estimated the top of the melting layer using the vertical gradients of MDV and reflectivity (White et al., 2002). Average MDV values just above this height were calculated for 30-min intervals concurrent with isotope samples. The top of the melting layer for periods of interest in this study was ~2 to 3 km above ground and the MDV values were adjusted for air density at that altitude.

Rio Claro: The precipitation events at Rio Claro were relatively short-lived and three events (8 October 2019, 10 December 2019 and 5 January 2020) had a sufficiently long stratiform period to allow averaging over 25- to 30-minute intervals. The top of the melting layer determined using the same approach as outlined above ranged from ~4 to 4.5 km and an altitude correction was applied to average MDV values.

2.3.4 Terminal fall velocity - MASC

The Multi-Angle Snowflake Camera (MASC) captures photographs of snow particles in free fall from multiple angles while simultaneously measuring their fall velocity (Garret and Yuter, 2014). The cameras are automatically triggered by near-infrared detectors that are vertically offset by 3.2 cm. The minimum particle size detected by the MASC is 0.1 mm. The fall velocity is calculated by the time difference when the upper and lower detectors are triggered successively within 1 s, equivalent to a minimum fall speed of 0.03 ms^{-1}.

At Summit, the MASC has operated since 2014 as a part of the ICECAPS observatory (Shupe et al., 2013). Measurements of fall velocity for several days in June, July and August 2014 were concurrent with isotope samples. Photographs of snow

https://doi.org/10.5194/egusphere-2026-687
Preprint. Discussion started: 5 March 2026

particles on which the fall velocity was measured provide visual evidence of the degree of riming corresponding to measured fall velocity. Note that the MASC measurements may not be fully representative of daily precipitation.

2.4 Snowflake photographs at Summit

An ice particle imaging camera (IcePIC), which consisted of a manually operated camera attached to a microscope, is a part of the instrument cluster of the ICECAPS observatory at Summit (Shupe et al., 2013). The device is housed in a wooden shed that prevents contamination from blowing snow during the collection of images. Falling snow was collected on glass slides that were cleaned with isopropyl/glycol mixture, dried, and placed on a wooden table. This table, however, was in an open area where blowing snow contamination on the slide was possible. To minimize this effect, the slides were placed on either side of a vertical barrier to be differentiated as upwind or downwind locations. Sample accumulation times ranged from a few minutes to several hours depending upon precipitation rate. The slides were then observed with the IcePIC system. The microscope stage and air around the device were at or near ambient temperature. The IcePIC photographs and accompanying notes from the microscopic examination were retrieved from the ICECAPS database (https://downloads.psl.noaa.gov/psd3/arctic/summit/icepic) on 31 July 2023. The photographs may be used to qualitatively characterize riming on ice crystals during precipitation events, but may not be representative of particle habits in all of the daily precipitation.

3 Results

We will first examine the correlation of d-excess with riming growth of ice in precipitation at Summit, Greenland using photographic images of snow particles, fall velocity measured with the MASC, and MDV. We will then discuss the d-excess and MDV correlations at other polar and non-polar locations in this study.

3.1 Riming and d-excess at Summit, Greenland

3.1.1 Snow particle photographs

We reviewed hundreds of IcePIC photos for the 2011-2014 period that were concurrent with the isotope samples. Selected images corresponding to a range of d-excess values in daily precipitation are shown in Table 3. High d-excess (~22‰) occurs in the summer (JJA) when snowfall contains unrimed single crystals or aggregates of various shapes, including columns, bullets, stellar plates or dendrites. Lower summer d-excess (~14‰) is associated with snow particles showing heavier riming. The original crystal shapes of stellar plates and dendrites are preserved but riming growth covers almost the entire particle surface.

https://doi.org/10.5194/egusphere-2026-687
Preprint. Discussion started: 5 March 2026

Lowest d-excess of –2.5 to +3.8‰ corresponds to winter snowfall (DJF) with relatively small particles of ~20 to ~700 µm. The smallest particles (~20 to 30 µm) appear to be frozen drops, likely broken off or splintered from ice particles where freezing would have initiated. As the IcePic photographs are based on snow particles collected on a slide kept in open air, blowing snow may have been captured and all of the small particles may not have fallen directly as precipitation.

3.1.2 MASC fall velocity

The MASC-measured average fall velocity of snow particles and the d-excess of corresponding daily samples of summer precipitation (JJA) are shown in Fig. 2. Representative photographs of snow particles, on which the fall velocity was measured, also are shown. The average fall velocity was calculated from 3 to 93 measurements, except for one sample that had a single measurement. Note that precipitation samples for d-excess were collected over an ~24 hr period while the MASC fall velocities were measured for shorter durations.

Although the MASC data are from the summer months (June – August), they correspond with a significant range of d-excess from +6.4 to +19.3‰. A strong, inverse correlation is seen between the d-excess of daily precipitation and the average fall velocity of snow particles (R^2 = 0.60; $p<0.01$). The particle shapes and riming in MASC photographs are consistent with those from the IcePIC photographs (Table 3). MASC photographs from two events in July (red triangles with d-excess of ~18‰; Fig. 2) show snow particles that are lightly rimed and the ice crystal shape is clearly evident. Following Locatelli and Hobbs (1974), these particles would be classified as lightly rimed assemblages of dendrites. The higher fall velocities (>1 ms^{-1}) and lower d-excess (~10‰) correspond to June events where heavily rimed particles have a more rounded shape with the underlying ice crystal outline no longer apparent. These particles would be classified as lump graupel or graupel-like snow (Locatelli and Hobbs, 1974). Near-ground MDV values greater than 1 ms^{-1} are known to indicate heavily rimed snow particles (Kneifel and Moiseev, 2020; Matrosov, 2023). For intermediate d-excess and fall velocities in July and August events, the particles are similar to lightly rimed aggregates of dendrites (Locatelli and Hobbs, 1974).

https://doi.org/10.5194/egusphere-2026-687
Preprint. Discussion started: 5 March 2026

Table 3. Photographs of snowflakes during precipitation events at Summit, Greenland captured with the IcePIC system. The scale bar in each photograph is ~500 µm (black) or ~100 µm (red).

			Date/Collector Notes	d-excess (‰) / MDV (ms^{-1})
A	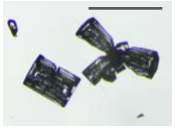	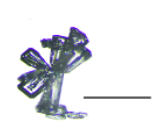	2012-07-03 Small columns, bullets and plates (not visibly rimed).	22.4 / 0.74
B		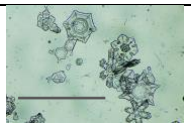	2012-07-24 Stellar crystals, small plates, dendrites (not visibly rimed).	22.7 / 0.53
C	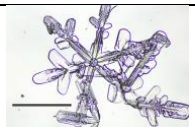	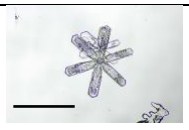	2012-06-25 Mostly aggregates. Stellar crystals, sectored plates (not visibly rimed).	21.4 / 0.66
D			2012-08-06 Moderately to heavily rimed stellar plates and dendrites.	13.8 / 1.1
E	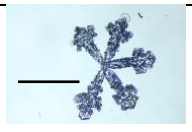	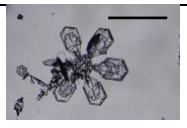	2012-05-27 Stellar dendrites and plates. Much riming, some very heavy. Unrimed particles (right) observed in the afternoon.	13.5 / 0.95
F	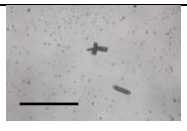	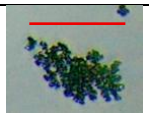	2014-01-06 Very small particles, columns, bullets and rosettes. (possible blowing snow contamination)	3.8 / 0.58
G	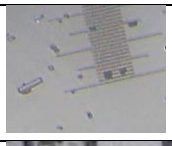	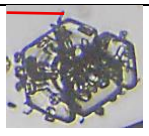	2014-02-05 Small needles, prisms, rime clumps, few plates with rime. (scale graduations: 0.01mm)	3.0 / 0.72
H			2014-01-29 Small columns, needles, prisms, large amount of rime pellets. (possible blowing snow contamination) (scale graduations: 0.01mm)	–2.0 / 0.80
I		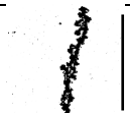	2014-02-28 Rimed crystals and smaller irregular crystals. Rime clump on right is magnified from a portion of the image on left.	–2.5 / 0.66

https://doi.org/10.5194/egusphere-2026-687
Preprint. Discussion started: 5 March 2026

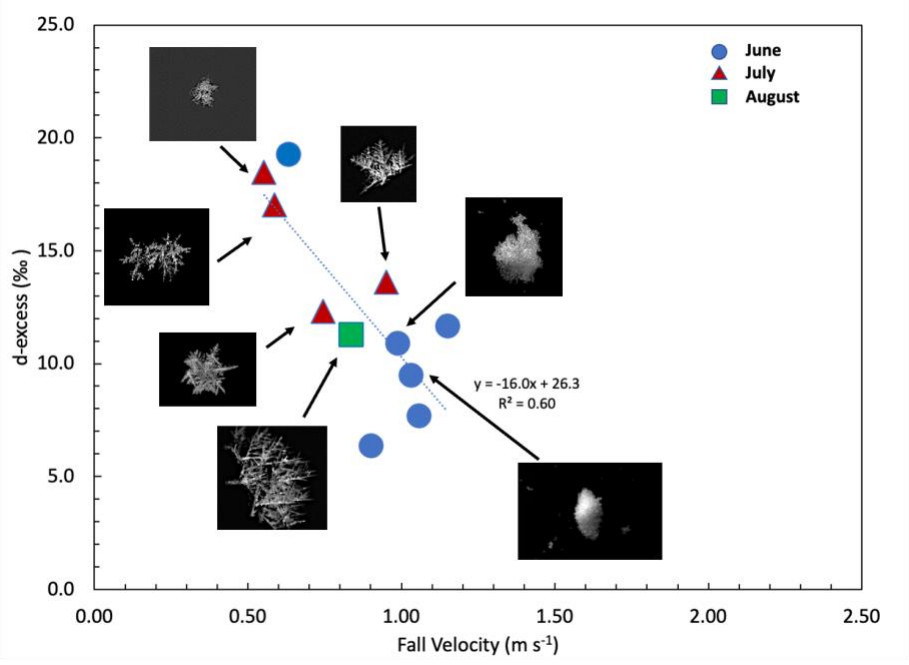

Figure 2. d-excess versus average fall velocity measured with a MASC at Summit. Selected photographs of particles for which the fall velocity was measured are also shown. The dotted line shows the best fit linear regression line.

3.1.3 Doppler velocity

Fig. 3 shows a scatter plot of d-excess versus MDV in daily precipitation at Summit. The data are categorized as summer (JJA) and winter (DJF). For clarity, Summit data for the other seasons are not shown as they lie within the bounds of the summer and winter categories (Fig. S4). We have also shown the MASC fall velocity data (from Fig. 2) for reference.

The variation of d-excess with MDV for the summer precipitation (blue circles in Fig. 3) shows essentially the same inverse relationship as that indicated by the MASC fall velocities (yellow circles in Fig. 3) also obtained in the summer. Samples with higher d-excess (>20‰) have a range of MDV values that are mostly less than ~0.9 ms^{-1}, indicating unrimed to moderately rimed particles (Locatelli and Hobbs, 1974). Lower d-excess of ~12 to 14‰ is associated with higher MDV (> 1 ms^{-1}) that is indicative of heavier riming (Kneifel and Moiseev, 2020; Matrosov, 2023). Table 3 shows a moderate to heavily rimed particle collected on 2012-08-06 when the d-excess and MDV values for daily precipitation were 13.8‰ and 1.1 ms^{-1}, respectively.

https://doi.org/10.5194/egusphere-2026-687
Preprint. Discussion started: 5 March 2026

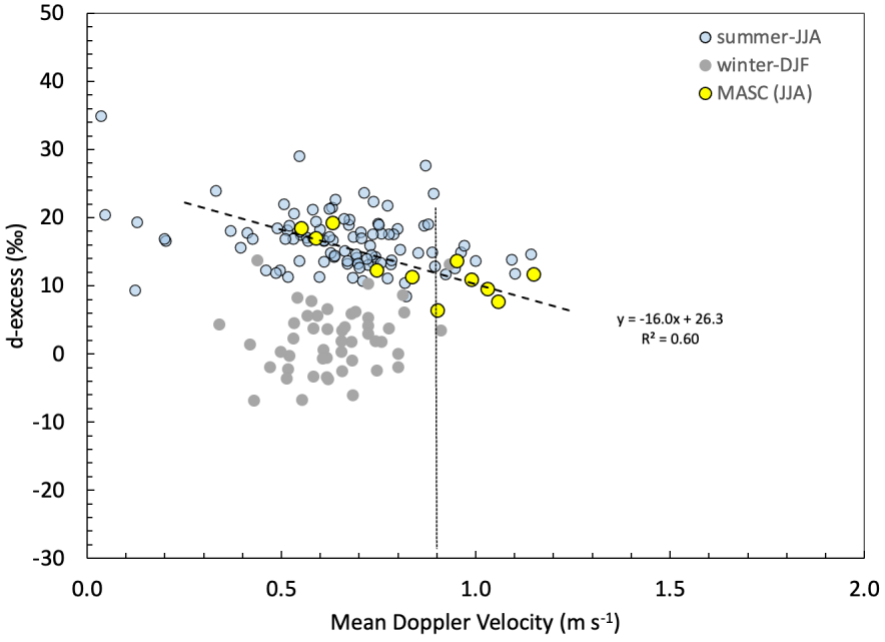

Figure 3. d-excess and MDV in daily precipitation at Summit, Greenland. The best fit line for the linear regression of d-excess and MASC fall velocities is shown (dashed line). The vertical dotted line shows the MDV of 0.9 ms^{-1}.

Samples of winter precipitation at Summit (gray circles in Fig. 3) mostly have lower d-excess than in the summer, but the MDVs are similar, albeit with a somewhat narrower range. This apparent lack of a relationship between d-excess and MDV in the winter may reflect differences in particle size and/or isotope fractionation compared to the summer. At colder temperatures, particle size is smaller (Heymsfield et al., 2013) and rimed particles or graupel are less dense (Garret and Youter, 2014), resulting in a generally lower fall velocity of rimed particles (Takahashi and Fukuta, 1988). This may mask an increase in winter MDVs due to riming (Kneifel and Moisseev, 2020; Matrosov, 2023). We can assess the particle size effect on MDV from differences in average Z_e for the summer (–5.7 dBZ) and winter (–14.3 dBZ). The Z_e and MDV values in our study are described by a power law with an exponent of 0.09, which is within the range of exponent values found for Arctic precipitation (Matrosov, 2023). These results suggest that, for similar levels of riming, the winter MDV values may be smaller by ~20% on average compared to the summer.

Alternatively, riming growth in the winter may occur on a nucleus consisting of a frozen drop, as opposed to a larger particle that formed by vapor deposition, resulting in a lower d-excess of the rimed ice. Experimental studies indicate that riming at low temperatures (–22 °C) can be initiated on particles as small as 30 to 60 µm (Avila et al., 2009). Clumps of frozen drops may be present in winter precipitation at Summit (e.g., Row I, Table 3), assuming that the image represents falling snow

https://doi.org/10.5194/egusphere-2026-687
Preprint. Discussion started: 5 March 2026

particles and not blowing snow. A proportionally smaller fraction of ice growth by vapor deposition in the winter compared to the summer may therefore result in much lower winter d-excess values. Additionally, Souchez and Jouzel (1984) found that ice formed by partial freezing had a lower d-excess as the initial $\delta^{18}O$ and $\delta^{2}H$ of the water decreased. Winter precipitation in general has lower $\delta^{18}O$ and $\delta^{2}H$ and the differences are starker in the polar regions. At Summit, the average winter ^{18}O and $\delta^{2}H$ are, respectively, –40‰ and –318‰, compared to –29‰ and –216‰ in the summer (Kopec et al., 2019). These large differences in seasonal isotopic compositions may result in a lower d-excess of rimed ice in the winter compared to the summer. We note that these explanations are somewhat speculative, although they are consistent with the generally lower particle size, reflectivity and MDV in the winter. A more detailed discussion of riming growth in the winter precipitation at Summit and its effect on d-excess is beyond the scope of this work.

Precipitation at Summit is attributed to deep (~ 4-6 km) or shallow (< ~3 km) clouds with varying proportions in different months (Shupe et al., 2013; Miller et al., 2015; Pettersen et al., 2018). Pettersen et al. used differences in the microwave absorption and scattering properties of cloud liquid water and ice to separate the majority of the precipitation events (both by accumulation and occurrence frequency) into three categories: snow originating from fully glaciated ice clouds (IC), snow where cloud liquid water was measurable in the column (CLW), and where the IC or CLW cloud types could not be differentiated based on their microwave signals (indeterminate). The CLW type clouds were single- or multi-layer, Arctic mixed-phase clouds while the IC type were similar to deep, nimbostratus-like clouds. Analysis of 36-hr back trajectories indicated that the CLW clouds frequently originated from the west-southwest of Greenland and the IC clouds primarily came from the southeast, but there were no seasonal differences in air mass trajectory for each of the cloud types. Snowfall mass accumulating at Summit from IC and CLW events was seasonally variable with CLW events more prevalent in the summer and the IC events in the winter (Pettersen et al., 2018). However, the indeterminate cloud type (that includes IC and CLW) had the same or higher accumulation in the winter as the IC type.

We used the results of Pettersen et al.'s classification, which was conducted at one minute time resolution, to calculate the mode of the cloud type at 12-hr intervals in daily precipitation. The dominant precipitating cloud type for low d-excess (–6.9 to 13.8‰) winter precipitation in this study is the indeterminate type (consisting of IC or CLW clouds) followed by the CLW type (Table S2). An examination of selected cloud radar images shows that supercooled liquid generally was present on days when d-excess was low and the indeterminate cloud type was dominant. This indicates that the indeterminate clouds for the winter days in our study likely were of CLW type, which would allow for the riming growth of ice.

https://doi.org/10.5194/egusphere-2026-687
Preprint. Discussion started: 5 March 2026

3.2 MDV and d-excess at other polar and non-polar locations

We now discuss the correlation of d-excess and MDV at Ny-Ålesund and Andenes (Norway), Dumont d'Urville (Antarctica), Cazadero (California), and Rio Claro (Brazil). Data for these locations are shown on Fig. 4 where we have also shown the Summit data (from Fig. 3) for reference. An inverse correlation of d-excess and MDV can be seen in Fig. 4. A linear regression of data from all locations, except Summit, suggests a fairly strong correlation (R^2 = 0.59, $p<0.01$) despite the wide differences in precipitation regimes, temperatures, and particle characteristics at these polar, mid-latitude and tropical locations. The correlation for individual locations also is fairly strong (R^2 = 0.43 to 0.78) except for Dumont d'Urville (R^2 = 0.18).

Ny-Ålesund precipitation samples (green circles in Fig. 4) consist both of snow and rain with a wide range of d-excess from –8.2 to +45.2‰. The corresponding MDV, at the 150 m level for snow and above the melting layer for rain, ranges from 0.6 to 1.8 ms^{-1}. The d-excess (–1 to 20.3‰) and MDV (0.7 to 1.1 ms^{-1}) values at Andenes (dark grey circles in Fig. 4) are similar to those at Ny-Ålesund.

Precipitation at Ny-Ålesund and Andenes occurs from low-level mixed-phase clouds within cyclonic, atmospheric river and frontal systems ((Lauer et al., 2023; Chellini and Kneifel, 2024; Ebell et al., 2024). Heavily rimed particles with higher MDVs are commonly observed at Ny-Ålesund (Chellini and Kneifel, 2024; Mahrendl et al., 2024). Riming results from increased turbulence, indicated by a higher eddy dissipation rate (EDR), which also is higher at cloud top temperatures warmer than about –10°C (Chellini and Kneifel, 2024), consistent with the generally lower d-excess of summer samples from Ny-Ålesund in our study.

Although the correlation at Dumont d'Urville (brown triangles in Fig. 4) is weak, the MDV values of ~1 to 1.8 ms^{-1} and lower d-excess of –2 to +14‰ are consistent with the common occurrence of graupel and other rimed particles in precipitation from synoptic, extra-tropical cyclones (Grazioli et al., 2017; Durán-Alarcón et al., 2019). For several samples in our limited dataset of 20 samples, MDV values of 1.5 to 1.8 ms^{-1} are higher than the maximum monthly average (~1.5 ms^{-1}) in a much larger, seven-year dataset of MDVs with 5500 measurements per month (Wiener et al., 2024). This may be an artefact of stronger turbulence in low-level katabatic winds so that the upward and downward air motions did not completely cancel out in our dataset (Sect. 2.3).

Cazadero and Rio Claro precipitation was sampled only as rainfall. Average MDVs were obtained over ~30 min intervals during stratiform events characterized by the presence of a reflectivity bright band. The top of the melting layer was at a height of ~2 km at Cazadero and ~4.5 km at Rio Claro. In the snow region above the melting layer, the average MDV and d-

https://doi.org/10.5194/egusphere-2026-687
Preprint. Discussion started: 5 March 2026

485 excess values, respectively, ranged from 0.9 to 1.9 ms^{-1} and –22.9 to +20.6‰ at Cazadero (open squares in Fig. 4) and from 1.2 to 1.6 ms^{-1} and +4.5 to +21.9‰ at Rio Claro (blue squares).

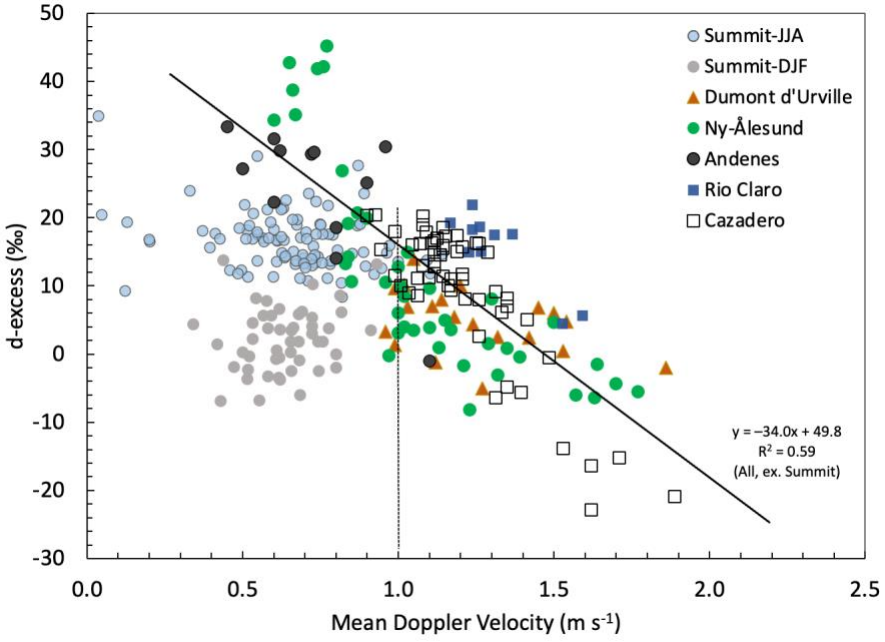

490 Figure 4. d-excess versus MDV in polar and non-polar precipitation. Summit data from Fig. 3 are shown for reference. The vertical dotted line marks the MDV value of 1.0 ms^{-1}. The best fit line for the linear regression, excluding Summit, is shown (solid black line). Regression of data from single locations (not shown) has R^2 values ($p<0.01$) of 0.43 (Andenes), 0.65 (Ny-Ålesund), 0.73 (Cazadero), 0.78 (Rio Claro) and 0.18 (Dumont d'Urville).

495

Stratiform precipitation at Cazadero is produced mostly in landfalling, extra-tropical cyclones and atmospheric rivers (White et al., 2003). Precipitation d-excess is nearly the same in both regimes (Coplen et al., 2015). Orographically forced, relatively deeper clouds at Cazadero seed the ice particles that fall through the lower, feeder clouds where water drops are accreted and ice grows by riming (White et al., 2003). At Rio Claro, precipitation is associated with mesoscale convective systems
500 (Santos et al., 2024) where the seeder–feeder process is commonly observed during stratiform events (Houze, 2014).

The bottom of the melting layer was at a height of ~1 km at Cazadero and ~4 km at Rio Claro and rainfall in the sub-cloud region may partially evaporate under unsaturated conditions. This evaporation would decrease the d-excess of precipitation collected on the surface compared to that in the snow region above the melting layer. Coplen et al. (2015) evaluated sub-

https://doi.org/10.5194/egusphere-2026-687
Preprint. Discussion started: 5 March 2026

cloud evaporation effects on d-excess in Cazadero precipitation and concluded that sub-cloud evaporation effects were not significant. We discuss the issue of sub-cloud evaporation and its effect on the inverse correlation of d-excess and MDV in more detail below.

3.3 Sub-cloud evaporation and d-excess

Sub-cloud evaporation decreases the drop size across the particle size spectrum although smaller raindrops evaporate faster (Kumjian and Ryzkhov, 2010; Xie et al., 2016). The decreased particle size would result in a decreasing reflectivity profile in the sub-cloud region and could be used as an indicator of rainfall evaporation.

The vertical profile of reflectivity below the melting layer during most of the precipitation events at Cazadero either did not decrease or decreased only for a brief interval at the beginning or the end of precipitation when rain rates generally were lower. In those cases, the d-excess and MDV data for about 30 min at the start or the end of an event were discarded to avoid the potential effect of sub-cloud evaporation on our analysis. This approach of partially discarding the early or late portions of an event was also used for Rio Claro.

However, decreasing reflectivity profiles in the sub-cloud region (Fig. S5) were present for several hours during one Cazadero precipitation event on 1 March 2009. The time-height profiles of reflectivity and MDV for this event are shown in Fig. S6. Precipitation began at about 03:00 UTC and continued through 24:00 UTC with several breaks in between. Lowest d-excess values at Cazadero, ranging from –22.9 to –13.9‰ (Fig. 4), were measured in the first three hours (05:45 to 08:45 UTC). The rain rate was < 1 mm hr^{-1} for most of this time interval (Coplen et al., 2015) and reflectivity profiles indicate that sub-cloud evaporation may have occurred.

The magnitude of the change in d-excess by sub-cloud evaporation was recently investigated by Graf et al. (2019). They assumed a cloud bottom at 1 km and surface relative humidity and temperature, respectively, of 75% and 12°C. In this scenario, a small raindrop (0.5 mm) may lose ~28% of its mass by sub-cloud evaporation that would lower its d-excess by ~10‰. For a larger drop (1 mm), ~7% of the mass may be lost with a 5‰ decrease in d-excess. For the 1 March 2009 Cazadero event, the sub-cloud region was about one km and the particle size was mostly greater than 0.5 mm (Fig. S7). We can consider that sub-cloud evaporation may have lowered the d-excess by a maximum of 5‰.

However, the MDV values in the snow region above the melting layer would be unaffected by any sub-cloud evaporation. An adjustment for sub-cloud evaporation would slightly increase the d-excess in the snow region, but that would only strengthen the inverse correlation with MDV (Fig. 4). Sub-cloud evaporation, therefore, would not be the primary factor responsible for the low d-excess of rainfall and its inverse correlation with MDV.

https://doi.org/10.5194/egusphere-2026-687
Preprint. Discussion started: 5 March 2026

The effect of sub-cloud rain evaporation on d-excess can also be evaluated by using the MDV observations immediately above and below the melting layer. As noted previously in Sect. 2.3.2, Weiss et al. (1977) have suggested that rimed and unrimed particles may be separated based on fall velocities in the snow region above the melting layer (V_s) and in the rain region immediately below (V_r). The proposed V_s – V_r categories for graupel, heavily rimed dendrites and aggregates of dendrites, as well as lightly rimed or unrimed particles are shown in Fig. 5. The variability of fall velocities within each category is quite large because of a range of particle size and density of the rimed and unrimed particles. If sub-cloud evaporation was responsible for the lower d-excess of rain, we would expect lower d-excess samples to lie in the unrimed or lightly rimed categories.

The V_s – V_r relationships in rainfall samples from Cazadero, Rio Claro and Ny-Ålesund also are shown on Fig. 5. Cazadero samples, for which the reflectivity profiles indicate potential sub-cloud evaporation, lie in the graupel or 'heavily rimed' aggregates fields (red squares). This is consistent with their low d-excess (–22.9 to –13.9‰) and the effect of sub-cloud evaporation, if any, would not have been significant. The rest of the Cazadero samples lie in the heavily- or moderately-rimed aggregates fields, consistent with their increasingly higher d-excess.

Two of the Rio Claro samples with low d-excess of +4.5 to +5.6‰ lie in the graupel field (large yellow squares in Fig. 5). Other Rio Claro samples have much higher d-excess, consistent with their location in the light to moderately rimed aggregates fields.

The d-excess of Ny-Ålesund samples is also consistent with their classification based on snow and rain region MDVs (Fig. 5). Lower d-excess samples lie in the graupel and heavily-rimed fields, consistent with a lack of sub-cloud evaporation as the bottom of the melting layer occurs within about 200 m above ground.

https://doi.org/10.5194/egusphere-2026-687
Preprint. Discussion started: 5 March 2026

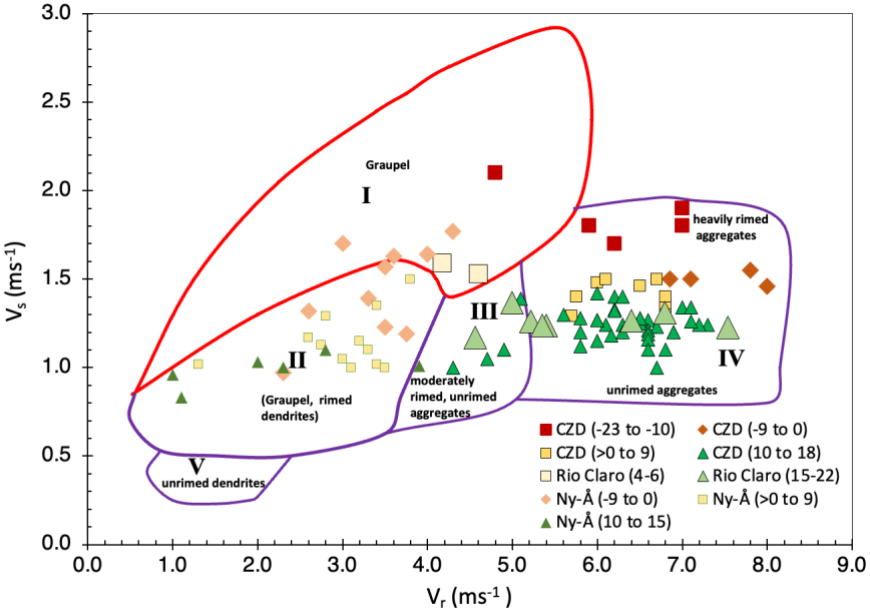

Figure 5. Classification of rimed and unrimed particles based on fall velocities above and below the melting layer. The boundaries for Categories I to V are as proposed by Weiss et al. (1977): **I.** Graupel (lump and conical, hexagonal) and graupel-like snow; **II**. Graupel, graupel-like snow, moderately to densely rimed dendrites, assemblages of dendrites, and columns, aggregates of unrimed side planes, bullets and columns; **III**. Moderately rimed to unrimed aggregates of dendrites; unrimed aggregates of bullets, side planes and columns; **IV**. Moderately rimed to unrimed aggregates and radiating assemblages of dendrites; **V**. Unrimed dendrites. Graupel with varying density plots in multiple fields (highest density in category I). For categories II, III and IV, unrimed particles plot towards the bottom and densely rimed towards the top. Also plotted are the rainfall samples from Cazadero (CZD), Rio Claro and Ny-Ålesund. The color and shape of symbols correspond to d-excess values as shown in the legend.

4 Discussion

We have used the MDV of snow particles during snow or rain precipitation as a proxy for riming. Its inverse correlation with the d-excess of precipitation collected on the surface in polar to tropical regions shows that isotopic fractionation occurs via riming and results in a lower d-excess of rimed ice compared to that of the liquid. This fractionation is opposite to that during ice growth by the WBF process where the ice phase has a higher d-excess.

The MDV can also be used to characterize the rimed mass fraction (RMF), the ratio of particle mass acquired by riming to the total mass, that is important for understanding the influence of microphysics on precipitation formation and the impact of

https://doi.org/10.5194/egusphere-2026-687
Preprint. Discussion started: 5 March 2026

climate change (Morrison et al., 2020). Improved simulations of future Greenland ice sheet melting and mass budget also require a better characterization of the liquid or ice phase of cloud particles (Morrison et al., 2020). A correlation of d-excess with RMF could be used to determine spatial and temporal patterns of RMF variations in modern precipitation and ice cores. The lower d-excess from riming would also help to explain the spatial variations of surface snow on Greenland and Antarctica that were previously attributed to changes in source moisture origin and reorganization of high-latitude hydrological cycles. The d-excess correlation with RMF and spatial variation of d-excess in the polar regions are discussed below.

4.1 Rimed mass fraction

Methods to calculate RMF from MDV have been proposed by Mosimann (1995) and Kneifel and Moisseev (2020). Mosimann (1995) used a vertically-pointing Doppler radar to measure the MDV of snow in the Swiss Alps. This was correlated with the RMF estimated from a visual analysis of individual snow particles (Mosimann et al., 1994). More recently, Kneifel and Moisseev (2020) used an extensive database of particle shapes, size, and fall velocities measured in precipitation at Hyytiälä, Finland to calculate the RMF. The rimed mass was calculated as the difference between the total mass and unrimed particle mass. The total particle mass was estimated from the fall velocity and mean particle mass for a given size bin (von Lerber et al., 2017). The unrimed mass was determined by assuming that the smallest 5% of the particles in each of the disdrometer's 0.2 mm size bins were unrimed (Moisseev et al., 2017). Using the measured particle size distribution, Kneifel and Moisseev (2020) calculated the expected MDV and a fourth-degree polynomial regression gave the best fit to the calculated RMF and MDV values. The relationship proposed by Kneifel and Moiseev reproduced well the RMF for the original data of Mosimann (1995). We have used the Kneifel and Moiseev (2020) method to calculate the RMF from MDV at all locations in our study.

Figure 6 shows a scatter plot of d-excess versus RMF. An inverse correlation is evident, similar to that with MDV, and d-excess decreases with an increasing RMF. We note that some of the RMF values for Summit and Ny-Ålesund are negative. This is an artefact of the generalized fall velocity – size relationship used in the formulation for unrimed particles. That, however, may not accurately define the relationship for unrimed particles in this study and result in negative RMF values (Kneifel and Moisseev, 2020).

A linear regression of d-excess and RMF from all locations, excluding Summit, shows a strong correlation (R^2 = 0.59; $p<0.01$). A correction for sub-cloud evaporation of some of the Cazadero and Ny-Ålesund samples would only make the correlation stronger because that would increase the d-excess without affecting the calculated RMF. We have excluded the Summit data from this regression because of the much lower d-excess values of winter precipitation. As discussed earlier (Sect. 3.1.3), this may result from riming in the much colder temperatures in polar winters. The regression equation indicates

https://doi.org/10.5194/egusphere-2026-687
Preprint. Discussion started: 5 March 2026

a low d-excess of about –39‰ for fully rimed particles (graupel at RMF = 1) and a high d-excess of about +30‰ for unrimed particles growing by vapor deposition (RMF = 0). These lower and upper bounds for d-excess are remarkably similar to the d-excess of precipitation on a daily or shorter time scale in the polar to tropical regions. For example, d-excess values ranging from –50 to +66‰ have been reported for daily or event-based precipitation at Dome F (Fujita et al., 2006) and Dome C (Schlosser et al., 2017) in eastern Antarctica, from –34 to +32‰ for Arctic precipitation in Alaska, USA (Bailey et al., 2019), from –26 to +30‰ in the mid-latitude precipitation in central USA (Tian et al., 2019), and from –28 to +29‰ in tropical precipitation at Mulu, Malaysia (Moerman et al., 2013).

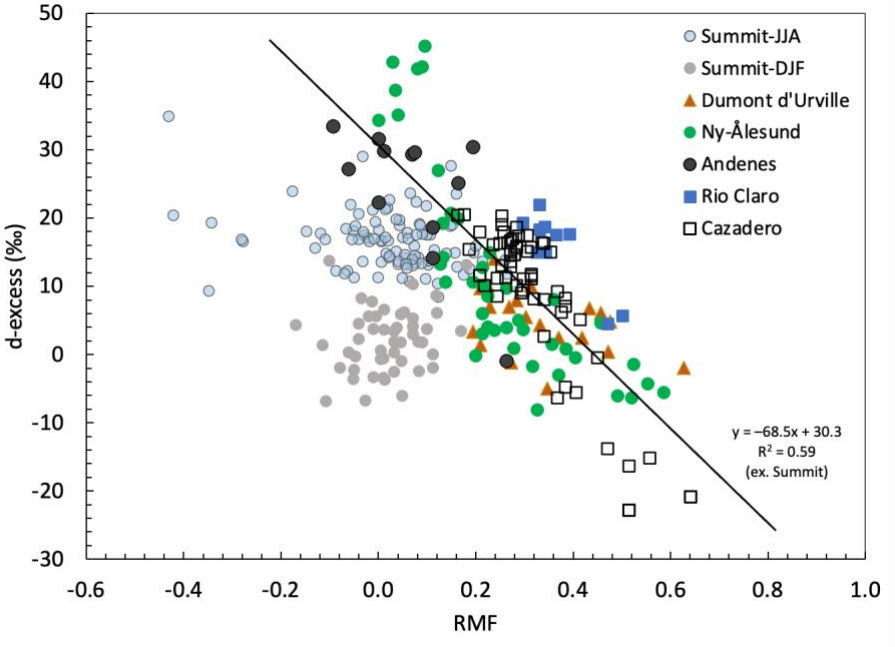

Figure 6. d-excess and rimed mass fraction (RMF) in this study. The RMF values were obtained using the method of Kneifel and Moisseev (2020). The solid black line is based on a regression of data from all locations except Summit. The negative values of RMF are an artefact of assumptions in model development (see text).

The inverse correlation of d-excess with RMF shows that the microphysical processes of ice growth in mixed-phase clouds (vapor deposition or riming) can result in both high and low d-excess of precipitation. These processes reflect dynamic forcing that may change rapidly and frequently during a precipitation event (Korolev et al., 2017). Consequently, precipitation collected on the ground even at a relatively short (10-20 min) time interval may contain hydrometeors that would have grown both by vapor deposition (WBF) and riming. This implies that the isotopic analysis of precipitation sampled on an hourly or daily scale would essentially provide a 'process-weighted' value of d-excess. That would explain

https://doi.org/10.5194/egusphere-2026-687
Preprint. Discussion started: 5 March 2026

the relatively large range of d-excess observed in daily or event-based precipitation (e.g., –50 to +60‰ at Dome C, Antarctica) while a seasonal or annual composite sample may have a very muted range (~10‰ in surface snow at Dome C; Wang et al., 2022). Further, a difference in d-excess over a long period, for example the lower d-excess of ice cores from the LGM compared to the Holocene (Jouzel et al., 2007), could be reconciled as a result of persistent changes in cloud processes rather than hydrological conditions.

4.2 Spatial d-excess variations

As we have noted previously, differences in source moisture origin that have conventionally been used to explain low d-excess of precipitation, may only have a limited influence because most precipitation on Earth originates as snow (Mülmenstädt et al., 2015). We have discussed below the spatial d-excess variations of surface snow on Antarctica and Greenland in the light of our results that precipitation d-excess reflects the process of ice growth (WBF and riming) in mixed phase clouds.

4.2.1 Antarctica

The d-excess of surface snow in Antarctica (Fig. 7) varies from values below zero to about +20‰ (Masson-Delmotte et al., 2008; Wang et al., 2022). Lower values generally are observed near the coast to about 800 km inland, and on the Antarctic Peninsula. Inland from the coastal areas, d-excess increases more or less linearly to about 2000 m altitude. We note that a much wider range of d-excess values (about –50‰ to +60‰) has been observed in daily precipitation at Dome C or Dome F on the Antarctic Plateau (Schlosser et al., 2017, Fujita et al., 2006).

Listowski et al. (2019) conducted a continent-wide study of tropospheric Antarctic clouds between 60° and 82° S latitudes using satellite-based cloud radars and lidars. Mixed-phase clouds with supercooled liquid were ubiquitous over Antarctica. The fraction of clouds with supercooled liquid in the coastal areas of east Antarctica was as high as ~40% in the summer and decreased sharply poleward with increasing surface elevation to ~10% over the Antarctic Plateau. Ricaud et al. (2024) observed clouds with supercooled liquid over Dome C. This indicates the potential for widespread riming and correspondingly lower d-excess in east Antarctic precipitation, including at Dome C and Dome F. We note that the spatial distribution of liquid-containing clouds in Listowski et al. appears quite similar to the shape of d-excess variation displayed in Fig. 7.

We have previously described the association of lower d-excess with higher fall velocities and riming at the coastal location of Dumont d'Urville (Sect. 3.2). Likewise, moderate to heavy riming has been shown at McMurdo (Tridon et al., 2022) and in its vicinity at the Mario Zucchelli station (Scarchilli et al., 2020). At both of these locations, snow particle fall velocities

https://doi.org/10.5194/egusphere-2026-687
Preprint. Discussion started: 5 March 2026

are frequently greater than ~1 ms^{-1} near the surface, consistent with the low d-excess values resulting from more frequent heavier riming. Warburton (1978) noted that rimed ice crystals were dominant in falling snow near the McMurdo station and that their proportion decreased with distance from the coast as growth by vapor deposition became dominant in inland precipitation. Di Natale et al. (2022) have reported the occurrence of heavily rimed particles in Dome C precipitation, consistent with low d-excess observed in daily precipitation (Schlosser et al., 2017). Riming was also shown to be important for ice crystal formation on both sides of the Antarctic Peninsula (Lachlan-Cope et al., 2016) where the surface snow has low d-excess values (Fig. 7).

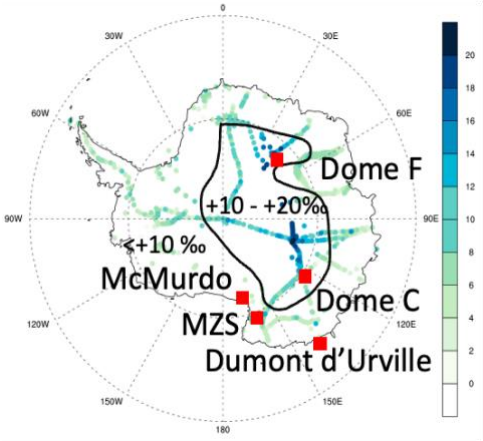

Figure 7. Spatial variation of d-excess of surface snow across Antarctica. The base map along with the small colored circles showing the measured d-excess values of surface snow were obtained from Wang et al. (2022). Red circles mark the locations of various research stations (MZS is Mario Zucchelli station). The thick black curve approximately traces the boundary between d-excess values less than or greater than 10.

Dütsch et al. (2019) simulated the spatial variation of d-excess over Antarctica with the isotope-enabled version of the community atmosphere model (iCAM5; Nusbaumer et al., 2017). That study simulated well the higher d-excess values resulting from ice growth by the WBF process. The low d-excess values however were substantially under-estimated. The isotopic scheme in iCAM5 includes isotopic fractionation for WBF, but not for riming (Nusbaumer et al., 2017; Dütsch et al., 2019). A sensitivity study of model parameters indicated that the under-estimation of lower d-excess was improved most by increasing the sedimentation velocity of ice particles (Dütsch et al., 2019). The sedimentation velocity in CAM5 results in changing the accretion rates and the proportion of ice formed by riming (Gettleman et al., 2015). It is likely, therefore, that modified isotope schemes that account for isotopic fractionation during riming growth will allow a more realistic simulation of isotopic variations over Antarctica.

https://doi.org/10.5194/egusphere-2026-687
Preprint. Discussion started: 5 March 2026

4.2.2 Greenland

The spatial variation of d-excess in surface snow over Greenland (Fig. 8) is characterized by relatively higher values in the north and northwest (e.g., Camp Century and NEEM) and lower values in the south-southeast (e.g., Dye 3). The sources of isotopic data shown on Fig. 8 are Osterberg et al. (2015; Camp Century), Landais et al. (2012; NEEM), Masson-Demotte et al. (2005; NGRIP and GRIP), Holme et al. (2019; Rennland), Johnson et al. (1989; Dye-3). In central Greenland, two locations that have been used extensively for ice core drilling – NGRIP and GRIP – are located only ~320 km apart, but the d-excess of surface snow is lower by ~1‰ at GRIP. Note that the GRIP site and Summit station are co-located on the Greenland central plateau.

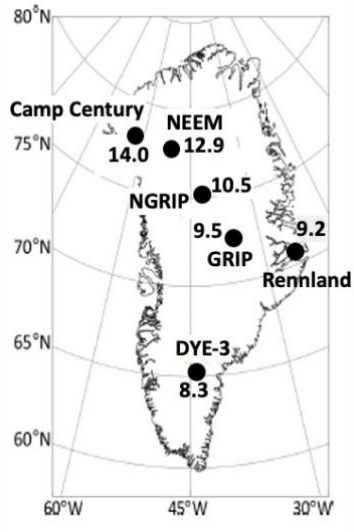

Figure 8. Spatial variations of d-excess in Greenland surface snow. The north-south locations are marked in black circles and the numbers show the d-excess value. The base map is from Rasmussen et al. (2023).

The d-excess differences across Greenland are observed in surface snow as well as in ice cores dating back to ~80,000 years (Masson-Delmotte et al., 2005; Jouzel et al., 2007). These differences have been attributed to different source moisture origins, source versus site temperatures, and snow formation by the WBF process under variable ice supersaturation conditions (Masson-Delmotte et al., 2005; Jouzel et al., 2007). Based on the results in this study, decreasing d-excess to the south may be attributed to increased riming.

McIlhattan et al. (2020) used space-borne cloud radar and lidar data, and the method proposed by Pettersen et al. (2018) for Summit, to calculate cloud types across the entire Greenland Ice Sheet. They concluded that all snow events across Greenland could also be attributed to the deeper IC clouds and the shallow CLW clouds. The air mass origin and transport

https://doi.org/10.5194/egusphere-2026-687
Preprint. Discussion started: 5 March 2026

characteristics from which CLW clouds originate in the west – southwest, and the IC clouds from the southeast in all seasons, were the same as at Summit. McIlhattan et al.'s classification used average annual values and the cloud type fractions varied geographically in the north-south and the east-west directions. In general, the fractions of both IC and CLW clouds increased towards the south, although the CLW to IC ratio decreased, suggesting that the CLW fraction was relatively lower in the south (Fig. S8). However, McIlhattan et al. noted that their approach based on space-borne radars under-estimated the CLW fraction by 25% compared to the surface-based approach of Pettersen et al. (2018). The IC clouds were under-estimated by only 5%. In addition, the indeterminate cloud type, which was the same or greater than the IC fraction in the winter at Summit, was not included in McIlhattan et al.'s classification.

Riming in southeastern Greenland precipitation at Dye-3 has been observed in the summer and the winter (Hogan et al., 1984; Davidson et al., 1989; Borys et al., 1993). In a detailed study over one year, Borys et al. found that 37% of the observed particles were lightly to moderately rimed such that the original particle shape was no longer visible. While riming was higher in warmer conditions, it was observed at temperatures as low as –34°C.

The changing cloud fractions from the north to the south and documented riming in the southernmost location of Dye-3 are consistent with the proposition that changing microphysical processes of ice growth result in decreasing d-excess from the north to the south of Greenland (Fig. 8).

5 Conclusions

The relative composition of oxygen and hydrogen isotopes or d-excess has been interpreted as an indicator of the climatic conditions (temperature, relative humidity, wind speed) during moisture origin at its source and/or as a consequence of kinetic isotope fractionation during snow formation by the vapor deposition process. Lower d-excess (<10‰) of precipitation is typically attributed to changes in source moisture origin and higher values to fractionation during snow formation. Because most precipitation on Earth originates as snow, the source moisture origin may only have a limited influence on d-excess and an alternative process must be responsible for the lower d-excess of precipitation.

In this study, we investigated the effect of the riming process of snow formation, where supercooled liquid droplets collide with falling ice particles in mixed-phase clouds and freeze directly on the particle surface, on the d-excess of ice. We used the terminal fall velocity of snow particles, measured with vertically-pointing Doppler radars, as an independent indicator of riming at several locations in the Arctic (Summit, Greenland, Ny-Ålesund, Svalbard and Andenes, Norway), Antarctic (Dumont d'Urville), mid-latitudes (Cazadero, California) and tropics (Rio Claro, Brazil). Concurrent measurements of d-excess and terminal fall velocity in daily or sub-daily precipitation are shown to be inversely correlated, except for the winter precipitation at Summit, Greenland. The d-excess in the winter precipitation at Summit is lower compared to the summer,

https://doi.org/10.5194/egusphere-2026-687
Preprint. Discussion started: 5 March 2026

while the terminal fall velocities are similar. This may be an artefact of smaller, less dense particles in the winter resulting in lower terminal fall velocity or a much lower d-excess in riming growth at colder temperatures. Excluding the data from Summit, a strong correlation ($R^2 = 0.59$) of d-excess and terminal fall velocity in precipitation from the rest of the polar and non-polar locations indicates robust dependence of d-excess on riming. This is the result of isotopic fractionation during riming by evaporation, and possibly partial loss of the accreted liquid by splashing and shedding, before freezing is complete. Isotopic fractionation during riming is contrary to the existing view, which holds that riming occurs without fractionation, but is consistent with previously published field, experimental, and modelling studies.

Consideration of lower d-excess resulting from riming helps to reconcile the spatial d-excess variations in surface snow observed across Greenland and Antarctica. In Greenland, increased riming to the south likely results in lower d-excess values. Similarly, lower d-excess in the coastal areas and higher values inland on Antarctica, which have been thus far difficult to explain based on source moisture origins, are consistent with increased riming in the coastal areas.

Although our study focused on stratiform precipitation in order to allow the use of terminal fall velocity as an indicator of riming, the results are applicable for interpreting the lower d-excess of all precipitation. In particular, the lower d-excess of precipitation that is conventionally attributed to sub-cloud evaporation in mid-latitude and tropical precipitation likely results instead from riming with only a minor contribution from sub-cloud evaporation.

The fraction of snow particle mass attributed to riming (RMF) was calculated by using the terminal fall velocity and a strong inverse correlation is also shown between d-excess and RMF. Therefore, d-excess variations in precipitation and ice cores can be used to characterize RMF and its spatial or temporal variability.

One of the largest uncertainties in characterizing the impact of climate change arises from our limited understanding of the influence of microphysics on precipitation formation (Morrison et al., 2020). The isotope-based estimates of RMF suggested above should provide observational inputs for constraining microphysics schemes in climate models.

Data availability

All data used in this study were obtained from published sources or public databases, as cited in the text.

Supplement link

Supplementary material is provided in a separate file.

https://doi.org/10.5194/egusphere-2026-687
Preprint. Discussion started: 5 March 2026

Author contributions

PKA conceived the project and designed the methodology, compiled isotope and radar data, and conducted the analyses; CS, FJL and MDS contributed to refining the methodology; AF assisted in processing radar data; PKA wrote the original draft; CS, FJL and MDS critically reviewed and edited the original draft; PKA prepared the final manuscript.

Competing interests

There are no competing interests

Acknowledgements

The senior author expresses his sincere gratitude to the researchers who diligently collected and made publicly accessible the isotope and radar data utilized in this study, and to Jean Jouzel for his review of an earlier version of the manuscript. A. White of NOAA and V. Santos of UNESP, Rio Claro, kindly shared the radar data from Cazadero and Rio Claro electronically. MDS was supported by the National Science Foundation (OPP-2137091) and NOAA Cooperative Agreement (NA22OAR4320151).

References

Atlas, D., Srivastava, R. C. and Sekhon, R. S.: Doppler radar characteristics of precipitation at vertical incidence. Rev. Geophys., 11, doi:10.1029/rg011i001p00001, 1973.

Atmospheric Radiation Measurement (ARM) user facility: Millimeter Wavelength Cloud Radar (MMCRMOM). 2010-06-01 to 2017-09-01, Summit Station, Greenland (SMT) External Data (satellites and others) (X1). Compiled by N. Bharadwaj. ARM Data Center. Data set accessed 2023-03-27 at http://dx.doi.org/10.5439/1025228, 2010.

Atmospheric Radiation Measurement (ARM) user facility: Active Remote Sensing of CLouds (ARSCL) product using Ka-band ARM Zenith Radars (ARSCLKAZR1KOLLIAS), 2020-02-22 to 2020-03-24, ARM Mobile Facility (ANX) Andenes, Norway; AMF1 (main site for COMBLE) (M1). Compiled by K. Johnson, M. Jensen and S. Giangrande. ARM Data Center. Data set accessed 2026-01-17 at http://dx.doi.org/10.5439/1228768, 2019.

https://doi.org/10.5194/egusphere-2026-687
Preprint. Discussion started: 5 March 2026

Ávila, E. E., Castellano, N. E., Saunders, C. P. R., Bürgesser, R. E. and Aguirre Varela, G. G.: Initial stages of the riming process on ice crystals. Geophys. Res. Lett. 36, L09808, 2009.

Bailey, A., Noone, D., Dee, S.G., Nusbaumer, J., Conroy, J.L., Stevenson, S. and Atwood, A.: Toward a process-oriented understanding of water in the climate system: recent insights from stable isotopes, Env. Res.: Climate 4 012002, do1:10.1088/2752-5295/ada17b, 2025.

Bailey, H.L., Klein, S.L. and Welker, J.M.: Synoptic and mesoscale mechanisms drive winter precipitation $\delta^{18}O/\delta^{2}H$ in south-central Alaska, J. Geophys. Res., Atmospheres 124, no. 7 (2019): 4252-4266.

Bailey, I. H., Hulston, J. R., Macklin W. C. and Stewart, J. R.: On the isotopic composition of hailstones. Jour. Atm. Sci. 26, 689-694, 1969.

Casado, M., Cauquoin, A., Landais, A., Israel, D., Orsi, A., Pangui, E., Landsberg, J., Kerstel, E., Prie, F. and Doussin, J.-F.: Experimental determination and theoretical framework of kinetic fractionation at the water vapour–ice interface at low temperature, Geochim. Cosmochim. Acta, 174, 54-69, 2016.

Castellani, B. B., Shupe, M. D., Hudak, D. R. and Sheppard, B. E.: The annual cycle of snowfall at Summit, Greenland. J. Geophys. Res.: Atm., 120, 6654-6668, 2015.

Chellini, G. and Kneifel, S.: Turbulence as a key driver of ice aggregation and riming in Arctic low-level mixed-phase clouds, revealed by long-term cloud radar observations, Geophys. Res. Lett. 51, e2023GL106599, 2024.

Ciais, P. and Jouzel J.: Deuterium and oxygen 18 in precipitation: Isotopic model, including mixed cloud processes. J. Geophys. Res.: Atm. 99, 16793-16803, 1994.

Coplen, T. B., Neiman, P. J., White, A. B. and Ralph,F. M.: Categorization of northern California rainfall for periods with and without a radar bright band using stable isotopes and a novel automated precipitation collector, Tellus B: Chem. Phys. Met. 67, 28552 -28574, 2015.

Dansgaard, W.: Stable isotopes in precipitation,Tellus 16, 436-468, 1964.

Dansgaard, W., Johnsen, S. J., Møller, J. and Langway, C. C. Jr.: One thousand centuries of climatic record from Camp Century on the Greenland ice sheet, Science 166, 377-381, 1969.

https://doi.org/10.5194/egusphere-2026-687
Preprint. Discussion started: 5 March 2026

Davidson, C. I., Harrington, J. R., Stephenson, M. J., Small, M. J., Boscoe, F. P. and Gandley, R. E.: Seasonal variations in sulfate, nitrate and chloride in the Grennland ice sheet: Relation to atmospheric concentrations, Atm. Env., 23, 2483-2493, 1989.

Demoz, B. B., Warburton, J. A. and R. H. Stone: The influence of riming on the oxygen isotopic composition of ice-phase precipitation, Atmos. Res. 26, 463-488, 1991.

Di Natale, G., Turner, D. D., Bianchini, G., Del Guasta, M., Palchetti, L., Bracci, A., Baldini, L., Maestri, T., Cossich, W., Martinazzo, M. and Facheris, L.: Consistency test of precipitating ice cloud retrieval properties obtained from the observations of different instruments operating at Dome C (Antarctica), Atm. Meas. Tech. 15, 7235-7258, 2022.

Durán-Alarcón, C., Boudevillain, B., Genthon, C., Grazioli, J., Souverijns, N., van Lipzig, P.M., Gorodetskaya, I. V. and Berne, A.: The vertical structure of precipitation at two stations in East Antarctica derived from micro rain radars, The Cryosph. 13, 247-264, 2019.

Dütsch, M., Blossey, P. N., Steig, E. J. and Nusbaumer. J. M.: Nonequilibrium fractionation during ice cloud formation in iCAM5: Evaluating the common parameterization of supersaturation as a linear function of temperature, Jour. Adv. Modeling Earth Sys. 11, 3777-3793, 2019.

Ebell, K., Walbröl, A. and Krobot, K.: Measurements of micro rain radar at AWIPEV, Ny-Ålesund (2017-2021), [Data set]. https://doi.org/10.1594/PANGAEA.958967, PANGAEA, 2023

Ebell, K., Buhren, C., Gierens, R., Chellini, G., Lauer, M., Walbröl, A., Dahlke, S., Krobot, P. and Mech, M.: Multi-year precipitation characteristics based on in-situ and remote sensing observations at Ny-Ålesund, Svalbard. EGUsphere 1-34, 2024.

Federer, B., Brichet, N. and Jouzel. J.: Stable isotopes in hailstones. Part I: The isotopic cloud model, J. Atm. Sci., 39, 1323-1335, 1982.

Field, P. R. and Heymsfield, A. J.: Importance of snow to global precipitation. Geophys. Res. Lett. 42, 9512-9520, 2015.

Fitch, K. E. and Garrett, T. J.: Graupel precipitating from thin Arctic clouds with liquid water paths less than 50 g m− 2, Geophys. Res. Lett. 49, e2021GL094075, 2022.

https://doi.org/10.5194/egusphere-2026-687
Preprint. Discussion started: 5 March 2026

Fujita, K. and Abe, O.: Stable isotopes in daily precipitation at Dome Fuji, East Antarctica, Geophys. Res. Lett., 33, L18503, 2006.

Garrett, T. J. and Yuter, S. E.: Observed influence of riming, temperature, and turbulence on the fallspeed of solid precipitation, Geophys. Res. Lett., 41, 6515-6522, 2014.

Gettelman, A., Morrison, H., Santos, S., Bogenschutz, P. and Caldwell, P. M.: Advanced two-moment bulk microphysics for global models. Part II: Global model solutions and aerosol–cloud interactions, J. Clim. 28, 1288-1307, 2015.

Graf, P., Wernli, H., Stephan, P. and Sodemann, H.: A new interpretative framework for below-cloud effects on stable water isotopes in vapour and rain, Atm. Chem. Phy., 19, 747-765, 2019.

Grazioli, J., Genthon, C., Boudevillain, B., Duran-Alarcon, C., Del Guasta, M., Madeleine, J.-B. and Berne, A.: Measurements of precipitation in Dumont d'Urville, Adélie Land, East Antarctica, The Cryos., 11, 1797-1811, 2017.

Harimaya, T. and Sato, M.: Measurement of the riming amount on snowflakes, J. Fac. Sci. Hokkaido University: Geophysics, 8, 355-366, 1989.

Holme, C., Gkinis, V., Lanzky M., Morris, V., Olesen, M., Thayer, A., Vaughn, B. H. and Vinther, B. M.: Varying regional δ 18 O–temperature relationship in high-resolution stable water isotopes from east Greenland, Clim. Past, 15, 893-912, 2019.

Heymsfield, A. J., Schmitt, C. and Bansemer, A.: Ice cloud particle size distributions and pressure-dependent terminal velocities from in situ observations at temperatures from 0 to− 86 C, J. Atm. Sci., 70, 4123-4154, 2013.

Heymsfield, A. J. and Kajikawa, M.: An improved approach to calculating terminal velocities of plate-like crystals and graupel, J. Atm. Sci., 44, 1088-1099, 1987.

Hogan, A. W., Barnard, S. C., Kebschull, K., Townsend, R., Samson, J. A.: Aerosol variation in the western hemisphere Arctic, J. Aerosol. Sci., 15, 13-33, 1984.

Houze Jr, R. A., Cloud dynamics. Vol. 104. Academic press, 2014.

https://doi.org/10.5194/egusphere-2026-687
Preprint. Discussion started: 5 March 2026

Johnsen, S. J., Dansgaard, W. and White, J. W. C.: The origin of Arctic precipitation under present and glacial conditions, Tellus B: Chem. Phys. Meteo., 41, 452-468, 1989.

Jouzel, J., Delaygue, G., Landais, A., Masson-Delmotte, V., Risi, C., Vimeux, F.: Water isotopes as tools to document oceanic sources of precipitation, Water Resources Res. 49, 7469-7486, 2013.

Jouzel, J. and Merlivat, L.: Deuterium and oxygen 18 in precipitation: Modeling of the isotopic effects during snow formation, J. Geophys. Res.: Atmospheres, 89-D7, 11749-11757, 1984.

Jouzel, J., Merlivat, L. and Federer, B.: Isotopic study of hail: The δD-δ18O relationship and the growth history of large hailstones, Quart. J. Royal Met. Soc., 111, 495-516, 1985.

Jouzel, J., Stiévenard, M., Johnsen, S. J., Landais, A., Masson-Delmotte, V., Sveinbjornsdottir, A., Vimeux, F., Von Grafenstein, U. and White J. W. C.: The GRIP deuterium-excess record, Quat. Sci. Rev. 26, 1-17, 2007.

Karrer, M., Dias Neto, J. von Terzi, L. and Kneifel S.: Melting behavior of rimed and unrimed snowflakes investigated with statistics of triple-frequency Doppler radar observations, J. Geophys. Res.: Atmospheres, 127, e2021JD035907, 2022.

Kneifel, S. and Moisseev., D.: Long-term statistics of riming in nonconvective clouds derived from ground-based Doppler cloud radar observations, J. Atm. Sci., 77, 3495-3508, 2020.

Kopec, B. G., Feng, X., Posmentier, E. S. and Sonder, L. J.: Seasonal deuterium excess variations of precipitation at Summit, Greenland, and their climatological significance, J. Geophys. Res.: Atmospheres 124, 72-91, 2019.

Korolev, A., McFarquhar, G., Field, P. R., Franklin, C., Lawson, P., Wang, Z., E. Williams et al.: Mixed-phase clouds: Progress and challenges, Meteo. Mon. 58, 5-1, 2017.

Kumjian, M. R. and Ryzhkov, A. V.: The impact of evaporation on polarimetric characteristics of rain: Theoretical model and practical implications, J. App. Meteo. Clim., 49, 1247-1267, 2010.

Lachlan-Cope, T., Listowski, C. and O'Shea, S.: The microphysics of clouds over the Antarctic Peninsula–Part 1: Observations, Atm. Chem. Phys.16, 15605-15617, 2016.

https://doi.org/10.5194/egusphere-2026-687
Preprint. Discussion started: 5 March 2026

Landais, A., Steen-Larsen, H. C., Guillevic, M., Masson-Delmotte, V., Vinther, B. and Winkler, R.: Triple isotopic composition of oxygen in surface snow and water vapor at NEEM (Greenland), Geochim. Cosmochim. Acta, 77, 304-316, 2012.

Lauer, M., Rinke, A., Gorodetskaya, I., Sprenger, M., Mech, M. and Crewell, S.: Influence of atmospheric rivers and associated weather systems on precipitation in the Arctic, Atm. Chem. Phys., 23, 15, 8705-8726, 2023.

Leroy-Dos Santos, C.: From atmospheric water isotopes measurement to firn core interpretation in Adelie Land: A case study for isotope-enabled atmospheric models in Antarctica: [Data set]. Zenodo. https://doi.org/10.5281/zenodo.7708489, 2023.

Leroy-Dos Santos, C.: A 4.5 year-long record of Svalbard water vapor isotopic composition documents winter air mass origin V1 [Data set]. Zenodo. https://doi.org/10.5281/zenodo.3689566, 2020.

Lin, Y. and Colle, B. A.: A new bulk microphysical scheme that includes riming intensity and temperature-dependent ice characteristics, Monthly Weather Rev., 139, 1013-1035, 2011.

Listowski, C., Delanoë, J., Kirchgaessner, A., Lachlan-Cope, T. and King, J.: Antarctic clouds, supercooled liquid water and mixed phase, investigated with DARDAR: geographical and seasonal variations, Atm. Chem. Phys., 19, 6771-6808, 2019.

Locatelli, J. D. and Hobbs, P. V.: Fall speeds and masses of solid precipitation particles, J. Geophys. Res. 79, 2185-2197, 1974.

Lowenthal, D. H., Borys, R. D., Cotton, W., Saleeby, S., Cohn, S. A. and Brown, W. O. J.:The altitude of snow growth by riming and vapor deposition in mixed-phase orographic clouds, Atm. Env., 45, 519-522, 2011.

Lowenthal, D., Gannet Hallar, A., McCubbin, I., David, R., Borys, R., Blossey, P., Muhlbauer, A., Kuang, Z. and Moore, M.: Isotopic fractionation in wintertime orographic clouds, J. Atm. Ocean. Tech., 33, 2663-2678, 2016.

Macklin, W. C. and Payne, G. S.: A theoretical study of the ice accretion process, Quart. J. Royal Meteo. Soc., 93, 195-213, 1967.

Maherndl, N., Moser, M., Lucke, J., Mech, M., Risse, N., Schirmacher, I. and Maahn, M.: Quantifying riming from airborne data during the HALO-(AC)3 campaign, Atmos. Meas. Tech., 17, 1475-1495, 2024.

https://doi.org/10.5194/egusphere-2026-687
Preprint. Discussion started: 5 March 2026

Masson-Delmotte, V., Landais, A., Stievenard, M., Cattani, O., Falourd, S., Jouzel, J., Johnsen S. J., White, J.W.C., Werner, M., Sveinbjörnsdottir, A. and Fuhrer, K.: Holocene climatic changes in Greenland: Different deuterium excess signals at Greenland Ice Core Project (GRIP) and NorthGRIP, J. Geophys. Res.: Atmospheres, 110-D14, 2005.

Masson-Delmotte, V., S. Hou, A. Ekaykin, J. Jouzel, A. Aristarain, R. T. Bernardo, D. Bromwich et al.: A review of Antarctic surface snow isotopic composition: Observations, atmospheric circulation, and isotopic modeling, J. Clim., 21, 3359-3387, 2008.

Matrosov, S. Y.: Frozen hydrometeor terminal fall velocity dependence on particle habit and riming as observed by vertically pointing radars, J. App. Meteo. Clim., 62, 1023-1038, 2023.

McIlhattan, E. A., Pettersen, C., Wood, N. B. and L'Ecuyer, T. S.: Satellite observations of snowfall regimes over the Greenland Ice Sheet, The Cryosph., 14, 4379-4404, 2020.

Mellat, M., Bailey, H., Mustonen, K.-R., Marttila, H., Klein, E. S., Gribanov, K., Bret-Harte M. S., et al.: Hydroclimatic controls on the isotopic (δ^{18}O, δ^{2}H, d-excess) traits of pan-Arctic summer rainfall events, Front. Earth Sci., 9, 651731, 2021.

Merlivat, L. and Jouzel, J.: Global climatic interpretation of the deuterium-oxygen 18 relationship for precipitation, J. Geophys. Res.: Oceans, 84-C8, 5029-5033, 1979.

Miller, N. B., Shupe, M. D., Cox, C. J., Walden, V. P., Turner, D. D. and Steffen, K.: Cloud radiative forcing at Summit, Greenland, J. Clim., 28, 6267-6280, 2015.

Mitchell, D. L., Zhang, R. and Pitter, R. L.: Mass-dimensional relationships for ice particles and the influence of riming on snowfall rates, J. App. Meteo. Clim., 29, 153-163, 1990.

Moerman, J. W., Cobb, K. M., Adkins, J. F., Sodemann, H., Clark, B. and Tuen, A. A.: Diurnal to interannual rainfall δ^{18}O variations in northern Borneo driven by regional hydrology, Earth Planet. Sci. Lett., 369, 108-119, 2013.

Moisseev, D., von Lerber, A. and Tiira, J.: Quantifying the effect of riming on snowfall using ground-based observations, J. Geophys. Res.: Atmospheres, 122, 4019-4037, 2017.

https://doi.org/10.5194/egusphere-2026-687
Preprint. Discussion started: 5 March 2026

Morrison, H., van Lier-Walqui, M., Fridlind, A.M., Grabowski, W.W., Harrington, J.Y., Hoose, C., et al.: Confronting the challenge of modeling cloud and precipitation microphysics, J. Adv. Modeling Earth Sys., 12, e2019MS001689, 2020.

Mosimann, L.: An improved method for determining the degree of snow crystal riming by vertical Doppler radar, Atm. Res., 37, 305-323, 1995.

Mosimann, L., Weingartner, E. and Waldvogel, A.: An analysis of accreted drop sizes and mass on rimed snow crystals, J. Atm. Sci., 51, 1548-1558, 1994.

Mülmenstädt, J., Sourdeval, O., Delanoë, J. and Quaas, J.: Frequency of occurrence of rain from liquid-, mixed-, and ice-phase clouds derived from A-Train satellite retrievals, Geophys. Res. Lett., 42, 6502-6509, 2015.

Nusbaumer, J., Wong, T. E., Bardeen, C. and Noone, D.: Evaluating hydrological processes in the Community Atmosphere Model Version 5 (CAM5) using stable isotope ratios of water, J. Adv. Modeling Earth Sys., 9, 949-977, 2017.

Ohtake, T.: Observations of size distributions of hydrometeors through the melting layer, J. Atm. Sci., 26, 545-557, 1969.

Ohtake, T.: Atmospheric ice crystals at the South Pole in summer, Antarct. J., 13, 174-175, 1978.

Orr, B. W. and Kropfli, R. A.: A method for estimating particle fall velocities from vertically pointing Doppler radar, J. Atm. Oceanic Tech.,16, 29-37, 1999.

Osterberg, E. C., Hawley, R. L., Wong, G., Kopec, B., Ferris, D. and Howley, J.: Coastal ice-core record of recent northwest Greenland temperature and sea-ice concentration, J. Glaciology, 61, 1137-1146, 2015.

Pettersen, C., Bennartz, R., Merrelli, A. J., Shupe, M. D., Turner, D. D. and Walden, von P.: Precipitation regimes over central Greenland inferred from 5 years of ICECAPS observations, Atm. Chem. Phys., 18, 4715-4735, 2018.

Pfahl, S. and Sodemann, H.: What controls deuterium excess in global precipitation? Climate of the Past 10, 771-781, 2014.

Praz, C., Roulet Y.-A. and Berne, A.: Solid hydrometeor classification and riming degree estimation from pictures collected with a Multi-Angle Snowflake Camera, Atm. Meas. Tech.,10, 1335-1357, 2017.

https://doi.org/10.5194/egusphere-2026-687
Preprint. Discussion started: 5 March 2026

Protat, A. and Williams, C. R.: The accuracy of radar estimates of ice terminal fall speed from vertically pointing Doppler radar measurements, J. App. Meteo. Clim., 50, 2120-2138, 2011.

Pruppacher, H. R. and Klett, J. D.: Microphysics of clouds and precipitation, Springer New York, DOI 10.1007/978-0-306-48100-0, 2010.

Rasmussen, S. O., Dahl-Jensen, D., Fischer, F., Fuhrer, K., Hansen, S. B., Hansson, M., Hvidberg, C. S. et al.: Ice-core data used for the construction of the Greenland Ice-Core Chronology 2005 and 2021 (GICC05 and GICC21), Earth Sys. Sci. Data Discuss., 15, 3351–33641, 2023.

Ricaud, P., Durand, P., Grigioni, P., Del Guasta, M., Camporeale, G., Roy, A., Attié, J.-L. and Bognar, J.: In situ observations of supercooled liquid water clouds over Dome C, Antarctica, by balloon-borne sondes, Atm. Meas. Tech., 17, 5071-5089, 2024.

Santos, V., Durán-Quesada, A. M. Sánchez-Murillo, R. and Gastmans, D.: High-frequency isotope compositions reveal different cloud-top and vertical stratiform rainfall structures in the inland tropics of Brazil, Geophys. Res. Lett., 51, e2024GL109886, 2024.

Scarchilli, C., Ciardini, V., Grigioni, P., Iaccarino, A., De Silvestri, L., Proposito, M., Dolci, S., et al.: Characterization of snowfall estimated by in situ and ground-based remote-sensing observations at Terra Nova Bay, Victoria Land, Antarctica, J. Glaciology, 66, 1006-1023, 2020.

Schlosser, E., Dittmann, A., Stenni, B., Powers, J. G., Manning, K. W., Masson-Delmotte, V. and Cagnati, V. M.: An., Grigioni, P., Scarchilli, C., The influence of the synoptic regime on stable water isotopes in precipitation at Dome C, East Antarctica, The Cryosphere, 11, 2345-2361, 2017.

Seidl, A. W., Johannessen, A., Dekhtyareva, A., Huss, J. M., Jonassen, M. O., Schulz, A., Hermansen, O., Thomas, C. K. and Sodemann, H.: The ISLAS2020 field campaign: Studying the near-surface exchange process of stable water isotopes during the arctic wintertime, Earth Sys. Sci. Data: Discussions, 2024.

Shupe, M. D., Turner, D. D., Walden, von P., Bennartz, R., Cadeddu, M. P., Castellani, B. B., Cox, C. J., et al.: High and dry: New observations of tropospheric and cloud properties above the Greenland Ice Sheet, Bull. Amer. Meteo. Soc., 94, 169-186, 2013.

https://doi.org/10.5194/egusphere-2026-687
Preprint. Discussion started: 5 March 2026

Shupe, M.D., Kollias, P., Poellot, M. and Eloranta, E.: On Deriving Vertical Air Motions from Cloud Radar Doppler Spectra. J. Atm. Ocean Tech., 25, 547-557, DOI: https://doi.org/10.1175/2007JTECHA1007.1, 2008.

Souchez, R. A. and Jouzel, J.: On the isotopic composition in δD and $\delta^{18}O$ of water and ice during freezing, J. Glaciology, 30, 369-372, 1984.

Takahashi, T. and Fukuta, N.: Supercooled cloud tunnel studies on the growth of snow crystals between –4 and –20°C, J. Met. Soc. Japan, 66, 841-855, 1988.

Tian, C., Wang, L., Kaseke, K. F. and Bird, B. W.: Stable isotope compositions (δ2H, δ18O and δ17O) of rainfall and snowfall in the central United States. Sci. Rep. 8, 6712, 2018.

Tridon, F., Silber, I., Battaglia, A., Kneifel, S., Fridlind, A., Kalogeras, P. and Dhillon, R.: Highly supercooled riming and unusual triple-frequency radar signatures over McMurdo Station, Antarctica, Atm. Chem. Phys., 22, 12467-12491, 2022.

Uemura, R., Matsui, Y., Yoshida, N., Abe, O. and Mochizuki, S.: Isotopic fractionation of water during snow formation: Experimental evidence of kinetic effect, Polar Meteo. Glaciology, 19, 1-14, 2005.

von Lerber, A., Moisseev, D., Bliven, L. F., Petersen, W., Harri, A-M. and Chandrasekar, V.: Microphysical properties of snow and their link to Z e–S relations during BAECC 2014, J. App. Meteo. Clim., 56, 1561-1582, 2017.

Wang, J., Pang, H., Wu, S., Schoenemann, S. W., Uemura, R., Ekaykin, A., Werner, M., et al.: The Ant-Iso dataset: a compilation of Antarctic surface snow isotopic observations, Earth Sys. Sci. Data: Discussions, 2022.

Warburton, J. A.: Atmospheric processes and the chemistry of snow on the Ross Ice Shelf, Antarctica, J. Glaciology, 20, 149-162, 1978.

Weiss, R. R., Locatelli, J. D. and Hobbs, P. V.: Deduction of ice particle types in the vicinity of the melting layer from Doppler radar measurements, J. App. Meteo. Clim.,16, 314-316, 1977.

Weiss, R. R. and Hobbs, P. V.: The use of a vertically pointing pulsed Doppler radar in cloud physics and weather modification studies, J. App. Meteo. Clim., 14, 222-231, 1975.

https://doi.org/10.5194/egusphere-2026-687
Preprint. Discussion started: 5 March 2026

White, A. B., Gottas, D. J., Strem, E. T., Ralph, F. M. and Neiman, P. J.: An automated bright band height detection algorithm for use with Doppler radar spectral moments, J. Atm. Oceanic Tech., 19, 687-697, 2002.

White, A. B., Neiman, P. J., Ralph, F. M., Kingsmill, D. E. and Persson, P. O. G.: Coastal orographic rainfall processes observed by radar during the California Land-Falling Jets Experiment, J. Hydrometeo., 4, 264-282, 2003.

Wiener, V., Roussel, M.-L., Genthon, C., Vignon, É., Grazioli, J. and Berne A.: A 7-year record of vertical profiles of radar measurements and precipitation estimates at Dumont d'Urville, Adélie Land, East Antarctica, Earth Sys. Sci. Data, 16 821-834, 2024.

Xie, X., Evaristo, R., Troemel, S., Saavedra, P., Simmer, C. and Ryzhkov A.: Radar observation of evaporation and implications for quantitative precipitation and cooling rate estimation, J. Atm. Oceanic Tech., 33, 1779-1792, 2016.

Zawadzki, I., Szyrmer, W., Bell, C. and Fabry, F.: Modeling of the melting layer. Part III: The density effect, J. Atm. Sci., 62, 3705-3723, 2005.